Multi-Frequency Satellite Approaches for Snow on Sea Ice

Polar+ Snow on Sea Ice (PSSI)

Deliverable 3.1:

Algorithm Theoretical Baseline Document 2 (ATBD-2)

FMI

UNIVERSITY OF LEEDS

This page has been intentionally left blank

Document History

Version	Date	Updated by	Reason
1.a	*06/03/2022*	*All*	
1.b	*19/05/2023*	*JL, AC*	Update to Version 2 after algorithm evolutions

Detailed History of Changes

Version	Section	Updated by	Details
1.b		*JL, AC*	Addition of LEGOS algorithm for KuLa snow depth retrievals, and updates to other algorithms

Contact details: Dr. Jack Landy

CIRFA

UiT – The Arctic University of Norway

P.O. Box 6050 Langnes

NO-9037 Tromsø

Norway

jack.c.landy@uit.no

Dr. Florent Garnier

florent.garnier@legos.obs-mip.fr

Dr. Isobel Lawrence

I.R.Lawrence@leeds.ac.uk

The project website is http://www.cpom.ucl.ac.uk/snow-on-sea-ice/index.html

printed on Tuesday, May 30, 2023

Table of Contents

Table of Contents 5
1 Introduction 11
1.1 Document Structure 11
1.2 Document Status 11
2 Motivation 12
2.1 Role of snow in sea ice thickness retrievals 12
2.2 Project objectives 14
2.3 Document objectives 15
3 Prototype Ku Radar – Ka Radar (KuKa) snow thickness retrieval algorithms 17
3.1 Bias correction methodology (Guerreiro et al., 2016; Garnier et al., 2021) 17
3.1.1 Datasets 17
3.1.2 Snow thickness algorithm 17
3.1.3 Uncertainty budget 20
3.1.4 Latest developments 21
3.2 Calibration methodology (Lawrence et al., 2018) 21
3.2.1 Datasets 21
3.2.2 Snow thickness algorithm 21
3.2.3 Uncertainty budget 24
3.2.4 Latest developments 26
3.3 Waveform modelling methodology 27
3.3.1 Datasets 27
3.3.2 Snow thickness algorithm 27
3.3.3 Uncertainty budget 32
3.3.4 Latest developments 34
4 Prototype Ku Radar – Laser (KuLa) snow thickness retrieval algorithms 35
4.1 LEGOS methodology 35
4.1.1 Datasets 35
4.1.2 Snow thickness algorithm 36
4.2 Calibration methodology (Lawrence et al., 2018) 39
4.2.1 Datasets 39
4.2.2 Snow thickness algorithm 39

4.2.3 Uncertainty budget 40
4.2.4 Latest developments 41
4.3 Waveform modelling methodology 41
4.3.1 Datasets 41
4.3.2 Snow thickness algorithm 41
4.3.3 Uncertainty budget 43
4.3.4 Latest developments 44
5 Summary 45
References 46

List of Figures

Figure 1 - Seasonal pan-Arctic snow thickness evolution for the Warren climatology (Warren et al, 1999) and the SNOWMODEL (Stroeve et al., personal communication) forced with two different reanalysis products. 12

Figure 2 - Schematics of the radar altimeter CryoSat-2 (top left) and laser altimeter ICESat-2 (top right). The sea ice thickness for varying radar (bottom-left) and laser (bottom-right) freeboard and snow depth. 13

Figure 3 - (a) Probability density functions of the 25-km gridded pan-Arctic sea ice thickness calculated using the same radar freeboards in March 2014, but two different snow depth maps: (i) the Langrangian snow evolution scheme SNOWMODEL-LG and (ii) the adapted Warren 1999 snow climatology. (b) The sea ice thickness calculated with SNOWMODEL-LG minus the sea ice thickness calculated with the Warren 1999 snow climatology..... 13

Figure 4 - OIB theoretical freeboard – CS2 freeboard vs CS2 PP for the calibration period 2011 - 2016. Linear regression coefficients (blue line) and standard error (shaded line) are shown in the inset. 14

Figure 5 – Schematic representation of the footprints of SARAL and CryoSat-2 in SAR and pLRM modes. The use of the CryoSat-2 pLRM data allows to have impacts of the surface roughness on the signal in better agreement with the SARAL LRM data. 18

Figure 6 – Schematic representation of the methodology to compute the dual frequency Ka-Ku Alti Snow depth data. 19

Figure 7 – Maps of the Altimetric Snow Depth (ASD) annual mean snow depth (a) and its uncertainties (b) in the Arctic for 2015. The annual mean snow depth map of the modified Warren-99 climatology (c) and its difference with the ASD product (ASD-W99m, map d) are also presented. 20

Figure 8 – NASA Operation IceBridge data utilised in the calibration method. The white circle marks 81.5º N, the latitudinal limit of the AltiKa and Sentinel-3 satellite orbits. 22

Figure 9 - Calibration functions for Ka (left) and Ku (right) satellite freeboards. For each satellite, the difference between the measured and "expected" freeboard (from OIB) is plotted as a function of Pulse Peakiness, a proxy for surface roughness. Grey shading around linear fit shows the ± 68% prediction interval, equating to 10/8cm for Ka/Ku. 23

Figure 10 – Original (middle) vs. calibrated (right) Ka (AltiKa) freeboard for example month of November 2020. Freeboards are calibrated as a function of pulse peakiness (left), via the linear regression function derived above (Figure 9a). 23

Figure 11 - Original (middle) vs. calibrated (right) Ku (CryoSat-2+Sentinel-3) freeboard for example month of November 2020. Freeboards are calibrated as a function of pulse peakiness (left), via the linear regression function derived above (Figure 9b)..... 23

Figure 12 - Monthly snow depths for November 2019 - April 2020, derived from the KuKa calibration method. 24

Figure 13 - Left: grid-averaged error on Ku-radar interpolated sea level anomaly (iSLA), considered a proxy for freeboard uncertainty. This along-track uncertainty, when gridded, reduces by 1N

where N is the number of tracks per grid cell (middle). Right: The reduced iSLA error, i.e. the uncertainty on satellite radar freeboard, for an example month of 202003. 25

Figure 14 - Monthly snow depth uncertainty by the KuKa calibration method, for winter 2019-20... 26

Figure 15 – Application of the Facet-Based Echo Model (FBEM) to forward simulate a CryoSat-2 return from sea ice topography based on Operation IceBridge (OIB) airborne laser scanner observations from the Lincoln Sea. (a) Snow surface elevation model from the OIB Airborne Topographic Mapper (ATM) showing the CryoSat-2 pulse limited footprint in black and the locations of two leads crossing the footprint in yellow. (b) Snow surface height distribution and best fitting Lognormal model. (c) Actual observed CryoSat-2 waveform from the footprint. (d) Simulated total CryoSat-2 waveform (blue) and estimated contributions from air-snow interface, snow volume scattering, snow-ice interface, and ocean lead reflections, with inset CryoSat-2 sensing parameters. From Landy et al. (2019). 28

Figure 16 – Comparison of Gaussian (normal) and Lognormal statistical models fit to the observed snow surface height distribution on sea ice from OIB ATM data at the scale of the CryoSat-2 footprint. (a) Snow surface elevation from the ATM over multi-year sea ice in the Central Arctic. (b) Observed elevation distribution from the ATM with best fitting normal and Lognormal models, including statistics from Kolmogorov–Smirnov tests, RMSE, and standard deviations (roughness) of the two model fits. (c) Data source location. From Landy et al. (2020). 28

Figure 17 – Radar echo simulations for a single scattering interface (snow or sea ice), with a Lognormal roughness height distribution and different roughness standard deviations, in (Left) Ku-band SAR-mode with radar sensing parameters from CryoSat-2 SIRAL and (Right) Ka-band LRM-mode with radar sensing parameters from AltiKa SARAL. 29

Figure 18 – Best fitting model echoes to observed radar waveforms from (Top Row) CryoSat-2 SAR-mode and (Bottom Row) AltiKa LRM-mode. The left-hand plots show model fits to characteristic diffuse-type waveforms returned from a rough sea ice or snow surface. The right-hand plots show model fits to characteristic specular-type waveforms returned from smooth ocean lead surfaces. The zero time marks the 'epoch' or radar retracking point, i.e. the mean level of the scattering surface. The free parameters optimized during waveform fitting are inset: A = normalized waveform amplitude, t_0 = time difference of epoch to the time at waveform peak power, σ = large scale surface roughness, s_rms = mm-cm radar-scale surface roughness. Adapted from Landy et al. (2020). 30

Figure 19 – Example of the CryoSat-2 and AltiKa radar freeboards obtained from physical-model waveform fitting in December 2019, with comparison to ICESat-2 laser freeboards. On the bottom row are two estimates for the snow depth obtained from a simple difference between KuKa freeboards and KuLa freeboards (see below), corrected for the delayed Ku-band wavespeed through the snow volume. A map of the difference between the two derived snow depth estimates is shown in the bottom left. 31

Figure 20 – Time series for the seasonal change in snow depth obtained from physical model-based KuKa radar freeboards over the 2019-20 sea ice growth/snow accumulation season. The envelopes represent +/- one standard deviation around the mean snow depth. 32

Figure 21 – Comparison of the gridded radar freeboards obtained from physical model waveform fitting applied to CryoSat-2 and AltiKa to laser freeboards obtained from ICESat-2 in December 2019. (Left) Freeboard distributions. (Middle) Derived snow depth distributions and the

distribution of gridded differences between AltiKa and ICESat-2. (Right) The AltiKa freeboards plotted as a ratio of the ICESat-2 freeboards. (Note that distributions only cover the coinciding region of observations between the three sensors south of 81.5N). 33

Figure 22 – The relationship between AltiKa surface roughness (left) and the apparent difference between Ka-band and laser freeboards from AltiKa and ICESat-2, respectively (right). The relationship is characterized from all measurements between Nov 2019 and Apr 2020. The systematic bias between AltiKa and ICESat-2 increases as a function of the derived Ka-band radar surface scattering roughness. 34

Figure *23 - Footprint details for CryoSat-2 and ICESat-2 missions* 36

Figure 24 - Maps of a) CryoSat-2 Freeboard using the SAMOSA+ retracker ; b) ICESat-2 Freeboard and c) resulting snow over January 2021 37

Figure 25 - Maps of CryoSat-2 freeboard using a) TMFRA50 and b) SAMOSA+. c) Difference between the freeboards. 38

Figure 26 - Monthly snow depths for November 2019 - April 2020, derived from the KuLa calibration method 40

Figure 27 – Snow depth derived from the KuLa algorithm over 2019-20 applying physical waveform fitting to CryoSat-2 and using the ICESat-2 data from NSIDC ATL20 Version 3. The grey contour in the November map marks all regions where the CryoSat-2 and ICESat-2 freeboards are within 5 cm of each other. 42

Figure 28 – Time series for the seasonal change in snow depth obtained from physical model-based CryoSat-2 Ku-band radar freeboards and ICESat-2 laser freeboards over the 2019-20 sea ice growth/snow accumulation season. The envelopes represent +/- one standard deviation around the mean snow depth. 43

Figure 29 – (a) The distribution of Ku-band radar freeboard from multiple processing algorithms: ESA Baseline-D (ESA_BD_GDR), the LEGOS using SAMOSA+ (LEGOS_SAM) and TFMRA50 retrackers (LEGOS_T50), CPOM, and the University of Bristol LARM retracker (UOB) next to the laser freeboard from ICESat-2 ATL10 product (IS2) for collocated tracks from the period between 1st Nov 2020 and 31st Dec 2020. (b) shows the geographical distribution of the mean freeboard differences for the same period. Courtesy of Antoine Laforge. 44

Figure 30 – Direct intercomparison between radar freeboards from CryoSat-2 and laser freeboards from ICESat-2 along aligned *Cryo2Ice* orbits, with the differences in freeboard between sensors illustrating the snow cover over multi-year and first-year ice. Courtesy of Antoine Laforge..... 45

List of Tables

Table 1 - Covariances between satellite freeboards and freeboard corrections, required for snow depth uncertainty calculation.26

Acronyms and Abbreviations

AltiKa – Ka-band Altimeter
AMSR-E - Advanced Microwave Scanning Radiometer - Earth Observing System
ATBD – Algorithm Theoretical Basis Document
AVHRR - Extended Advanced Very High Resolution Radiometer
AWI – Alfred Wegener Institute
CICE – The Los Alamos Sea Ice Model
CRREL - Cold Regions Research and Engineering Laboratory
CryoVEx - CryoSat Validation Experiment
CS2 – CryoSat-2
DuST – Dual-altimeter Snow Thickness
ECMWF – European Centre for Medium-range Weather Forecasts
Envisat – Environmental Satellite
EO – Earth Observation
ERS – European Remote Sensing Satellite
ESA – European Space Agency
EXPRO – Express Procurement
FBEM - Facet-Based numerical Echo Model
FMI – Finnish Meteorological Institute
FYI – First-Year Ice
GLAS – Geoscience Laser Altimeter System
IABP – International Arctic Buoy Program
IAR – Impact Assessment Report
ICESat – Ice, Cloud and land Elevation Satellite
IMB – Ice Mass-balance Buoy
ITT – Invitation To Tender
KO – Kick-Off
KuKa – Ku (radar) / Ka (radar) snow thickness product
KuLa – Ku (radar) / Laser snow thickness product
LEGOS - Laboratoire d'Etudes en Géophysique et Océanographie Spatiales
LIM – Louvain-la-Neuve Sea Ice Model
MAF – Management, Administrative and Financial proposal
MYI – Multi-Year Ice
NASA – National Aeronautics and Space Administration
NCEP – National Centers for Environmental Prediction
NSIDC – National Snow and Ice Data Centre
OIB - Operation IceBridge
PP – Project Partner
RA2 – Radar Altimeter 2
RB – Requirement Baseline
SAR – Synthetic Aperture Radar
SARAL – Satellite for Argos and AltiKa
SHEBA - Surface Heat Budget of the Arctic Ocean
SIPN – Sea Ice Prediction Network
SMOS - Soil Moisture and Ocean Salinity satellite
SnoDSI – SNOw on Drifting Sea Ice
SOW – Statement Of Work
SR – Scientific Roadmap
SSM/I - Special Sensor Microwave Imager
SSMIS – SSM/I Sounder
STSE – Support To Science Element
SWE – Snow Water Equivalent
TP – Technical Proposal
UiT – Arctic University of Norway
UCL – University College London
W99 – Warren et al. (1999) snow climatology
WP – Work Package
YOPP – Year of Polar Prediction

1 Introduction

1.1 Document Structure

This document describes the Algorithm Theoretical Basis for six different multifrequency approaches to retrieve snow thickness over all types of sea ice surfaces in the Arctic. This includes approaches for our two main streams of snow thickness product derived from: (1) from satellite Ku-band and Ka-band radar altimetry, and (2) from satellite Ku-band radar and laser altimetry, over the 'operational period' for polar altimetry from 2013 to present.

The goal of the ATBD V2 is to finalize the different processing methodologies after the experimental snow thickness datasets have been validated against a suite of independent observations (in situ, airborne and snow modelling products) and an optimal snow product has been identified in WP4.

Project requirements are described in D2.1 Requirement Baseline Document (RBD).

Dataset collection for this project is described in D2.2 Dataset User Manual.

Some information about error estimation of the products and comparisons to independent datasets are already discussed in this document, but have been further expanded upon in the validation report D3.2. (Delivered in WP4)

1.2 Document Status

This is the second version of the ATBD, issued as part of WP3 of Polar+ Snow on Sea Ice.

2 Motivation

2.1 Role of snow in sea ice thickness retrievals

The climate of the Arctic is changing rapidly with well documented repercussions on the sea ice extent, thickness, speed and ice age among other characteristics (Stroeve & Notz, 2018). Changes in the snow cover on the other hand remain harder to monitor with limited in-situ and airborne observations (Shalina et al, 2020) covering only parts of the Arctic basin and biased towards the spring season (see WP2). Webster et al (2014), compared over the central Arctic and Canadian archipelago the Warren climatology (Warren et al., 1999) of the 1950s-1990s to an updated climatology over the Operation IceBridge (OIB) period 2009-2013 and found a decline in snow depth of 37% and 50% over first year ice (FYI) and multi-year ice (MYI) respectively. This decline contrasts with very deep snow measured in the Atlantic sector during the N-ICE2015 campaign (Merkouriadi et al, 2017) while new in-situ snow measurements are currently being collected as part of the MOSAiC expedition.

Every year, snow accumulates on the surface of the sea ice cover from the end of the summer season (September) and the snow depth grows steadily until the end of winter when it stabilizes at roughly 20-30 cm up until the beginning of the melt season (May) (Figure 1). At that time, the melt of the entire snow layer happens suddenly over a period of less than 2 weeks leading to the formation of melt ponds and resulting in a significant decrease of the albedo at the surface of the ice throughout the summer season.

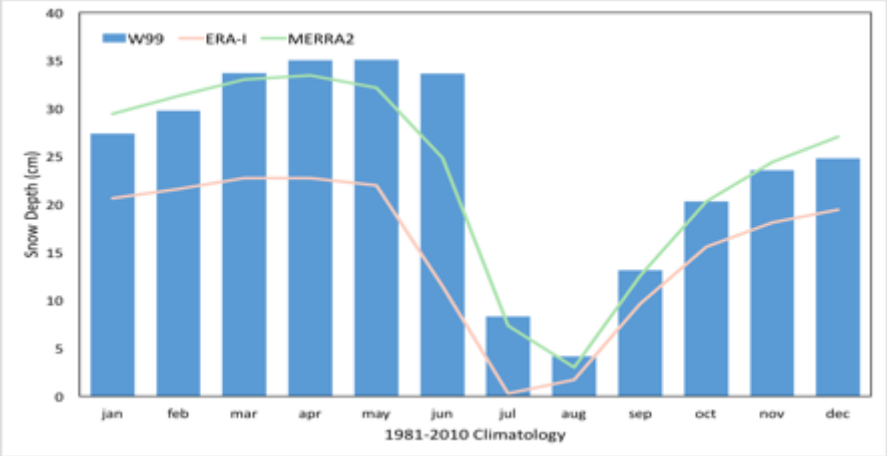

Figure 1 - Seasonal pan-Arctic snow thickness evolution for the Warren climatology (Warren et al, 1999) and the SNOWMODEL (Stroeve et al., personal communication) forced with two different reanalysis products.

All remotely sensed sea ice thickness data derived from laser or radar altimetry require auxiliary information about the snow accumulation upon ice. The snow depth and density needs to be estimated to account for the loading effect above the radar altimeter freeboard or to account for the portion of the laser altimeter freeboard that is snow rather than sea ice. Hence there is a distinct need to understand the depth, density and distribution and impact of snow on sea ice. The shift in the Arctic sea ice regime toward a predominantly seasonal ice pack also means that climatological snow information collected prior to the 1990s (e.g. Warren et al., (1999)) may not be as pertinent as it once was. Without sufficient knowledge of the snow cover, we cannot address important scientific questions such as the significance of sea ice mass decline as accurately as is necessary.

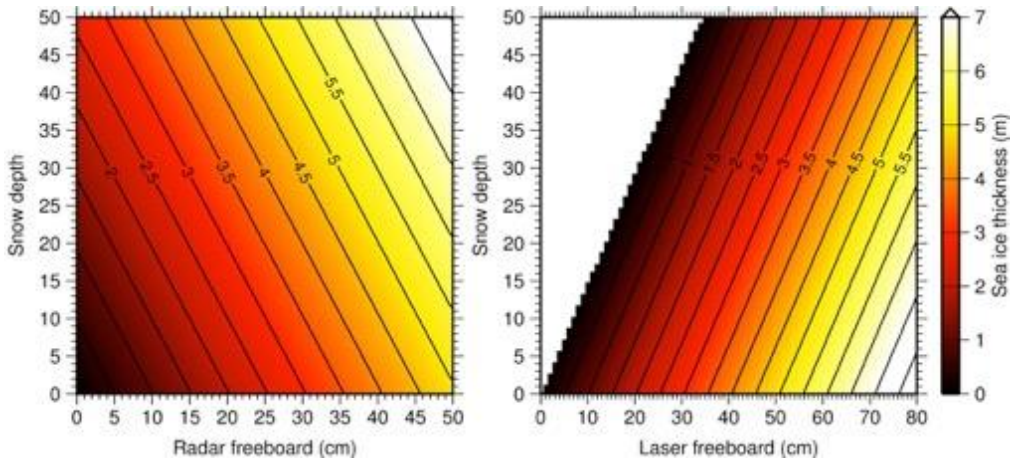

Figure 2 - Schematics of the radar altimeter CryoSat-2 (top left) and laser altimeter ICESat-2 (top right). The sea ice thickness for varying radar (bottom-left) and laser (bottom-right) freeboard and snow depth.

To illustrate the importance of snow depth for linking radar and laser altimeter-derived sea ice thickness, consider a sea ice floe with sea ice freeboard of 15cm and a snow layer depth of 20cm (Figure 2). For typical densities of sea ice, the ocean surface and snow of 920kgm^{-3}, 1024kgm^{-3} and 320kgm^{-3}, the sea ice thickness is 2.1m. However, if the snow layer depth is unknown and is taken to be a climatological value of, say, 30cm, the resulting thickness calculated from a laser altimeter will be 1.4m, and the thickness from a radar altimeter will be 2.6m.

One of the most significant limitations introduced by using the adapted Warren climatology to represent pan-Arctic snow depth on sea ice is the absence of spatiotemporal variability. Applying the adapted Warren snow depths to altimetry freeboard observations truncates the resulting sea ice thickness distribution, so that the mean ice thickness is approximately correct, but the quantities of thinnest and thickest ice are underestimated. Applying a numerical snow evolution scheme with more realistic spatiotemporal variability (SNOWMODEL-LG) to calculate pan-Arctic sea ice thickness leads to a much wider and more natural ice thickness distribution (Figure 3a). The differences in sea ice thickness estimated from Warren versus SNOWMODEL snow depths can be >1 m (Figure 3b).

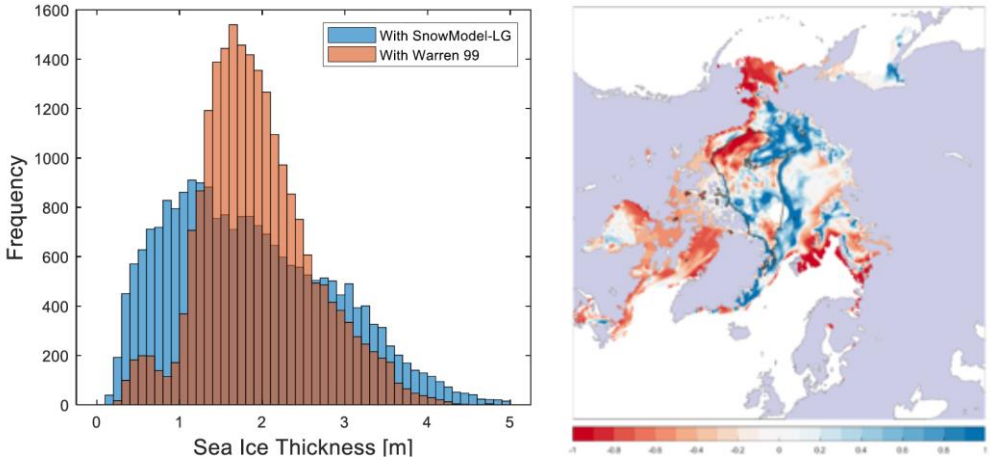

Figure 3 - (a) Probability density functions of the 25-km gridded pan-Arctic sea ice thickness calculated using the same radar freeboards in March 2014, but two different snow depth maps: (i) the Langrangian snow evolution scheme SNOWMODEL-LG and (ii) the adapted Warren 1999 snow climatology. (b) The sea ice thickness calculated with SNOWMODEL-LG minus the sea ice thickness calculated with the Warren 1999 snow climatology.

2.2 Project objectives

The primary objective of this project is to investigate multi-frequency approaches to retrieve snow thickness over all types of sea ice surfaces in the Arctic and provide a state-of-the-art snow product.

Our approach follows ESA ITT recommendations to prioritise satellite-based products and will benefit from the recent 'golden era in polar altimetry' with the successful launch of the laser altimeter ICESat-2 in 2018 complementing data provided by the rich fleet of radar altimeters, CryoSat-2, Sentinel-3 A/B, AltiKa. Our primary objective is to produce an optimal snow product over the recent 'operational' period.

This will be complemented by additional snow products covering a longer periods of climate relevance and making use of historical altimeters (Envisat, ICESat-1) and passive microwave radiometers for comparison purposes (SMOS, AMSRE, AMSR-2). In addition to snow thickness, and as a secondary objective, we will explore other snow characteristics (snow density, snow metamorphism, scattering horizon, roughness, etc) and compare these results with in-situ, airborne and other snow on sea ice products including from model studies and reanalysis on drifting sea ice products.

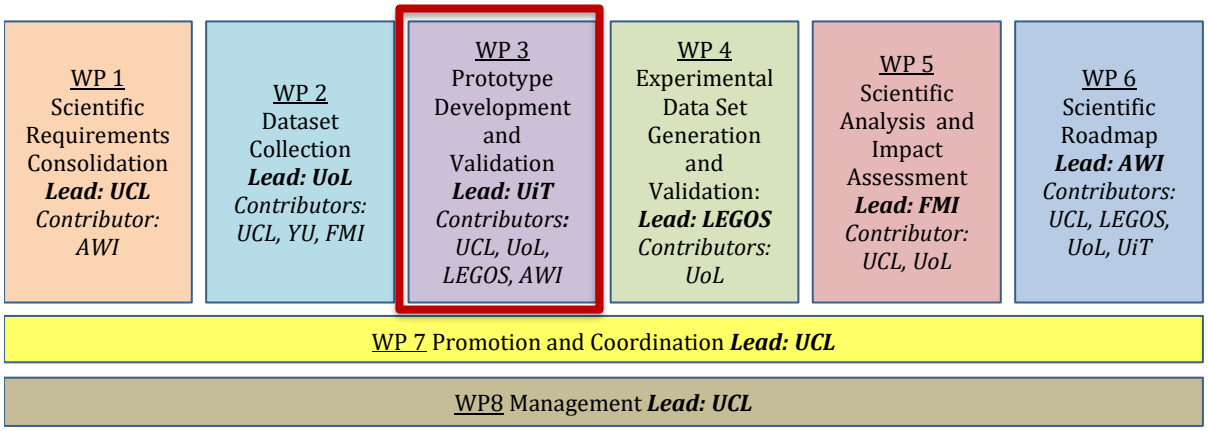

Figure 4 - OIB theoretical freeboard – CS2 freeboard vs CS2 PP for the calibration period 2011 - 2016. Linear regression coefficients (blue line) and standard error (shaded line) are shown in the inset.

The objectives of the Polar+ snow on sea ice activity are to:

- Better understand, quantify and document the snow depth penetration from laser, Ka and Ku band radar altimetry measurements function of the snow characteristics (density, temperature, salinity).
- Collect, analyse and exploit the most extensive multi-source in-situ and airborne datasets from EU (e.g., from ESA CryoVex airborne campaigns , MOSAIC …) and non -EU pan Arctic campaigns as well as existing long-term observations in order to confirm information content at each frequency and document validity and robustness of altimetry-based freeboard and snow-depth products.
- Generate improved multi-sensor snow depth products over the Artic Sea-ice for:
    - Altimetry-based sea-ice freeboard and thickness computation
    - Climate applications both related to the Cryosphere and the Polar Ocean thermohaline circulations

- Demonstrate the scientific impact of the generated product though a number of scientific studies focusing on major science questions in Arctic research where the snow on sea ice information may provide a novel contribution to science and open the door to potential future applications.
- Develop a scientific roadmap providing recommendations to ESA to further advance in the use of EO technology and satellite missions to address the main knowledge gaps and scientific challenges associated to snow on sea ice.

The Algorithm Theoretical Baseline Document addresses the first three of these objectives: (1) providing an improved understanding of multi-frequency radar scattering by snow and sea ice, (2) exploiting in-situ and airborne datasets from EU and non-EU field campaigns to develop new satellite snow depth products, and (3) describing the key methodologies we will use to generate an optimal altimetry-based sea-ice freeboard and snow depth product.

2.3 Document objectives

This document is our study's Deliverable 3.1, the Algorithm Theoretical Baseline Document (ATBD). It summarizes the results of WP3 of the study: developing the algorithms and prototype Multi-Frequency snow thickness and error analysis for our two main streams of radar-radar and radar-laser products. Following development of the methodology. It includes contributions from WP 3.1 "Development of prototype products and their validation Ku Radar – Ka Radar (KuKa) Algorithm: Development and Prototype" and WP 3.2 "Development of prototype products and their validation Ku Radar – Laser (KuLa) Algorithm: Development and Prototype". It lays the foundation for experimental dataset generation, validation, and identification of an optimal snow thickness product in WP4.

The WP3 tasks are broken down into the following sub-tasks:

WP3: Development of prototype products and their validation

- T3.1: Introduction to the document
- T3.2: Motivation for the project, project and document objectives
- T3.3: Prototype Ku Radar – Ka Radar (KuKa) snow thickness retrieval algorithms
- T3.4: Prototype Ku Radar – Laser (KuLa) snow thickness retrieval algorithms
- T3.5: Optimal interpolation algorithms for gridding data
- T3.6: Preliminary intercomparison of gridded data products
- T3.7: Outlook

Inputs required to Start:
• SoW [EOP-SDR/SOW/087-17/DFP]
• Proposal [UCL-PRO-19-MT1]
• Requirement Baseline Document [UCL_PRO_2020_1_MT]
• Dataset and Description Document [Polar+_D2.2_Dataset_Description_Document]
Task Description:
• WP 3.1.1 Radar freeboards —S. Fleury / I. Lawrence / M. Tsamados / J. Landy ○ LRM ○ SAR

- WP 3.1.2 Retrieving snow and ice freeboards
  - Calibration technique
  - Bias correction technique
  - Bias corrections
  - Uncertainties
- WP 3.1.3 Fusion algorithm – S. Fleury / I. Lawrence
- WP 3.1.4 Error analysis – S. Fleury / I. Lawrence / M. Tsamados
  - Modelling the snow pack characteristics – R. Mallett, M. Tsamados
  - Ka/Ku radar penetration into the snow - M. Tsamados, S. Fleury
  - Role of snow and ice roughness – J. Landy, M.Tsamados, S. Fleury

- WP 3.2.1 Laser freeboards — I. Lawrence / M. Tsamados / J. Landy / S. Hendricks
- WP 3.2.2 Retrieving snow and ice freeboards
  - Calibration technique
  - Bias correction technique
  - Bias corrections
  - Uncertainties
- WP 3.1.3 Fusion algorithm – I. Lawrence
- WP 3.1.4 Error analysis – I. Lawrence

-

Outputs:

- Contribution to D3.1.1 KuKa Algorithm Theoretical Baseline Document (ATBD-1)
- Contribution to D3.1.2 KuLa Algorithm Theoretical Baseline Document (ATBD-1)

3 Prototype Ku Radar – Ka Radar (KuKa) snow thickness retrieval algorithms

3.1 Bias correction methodology (Guerreiro et al., 2016; Garnier et al., 2021)

3.1.1 Datasets

The Altimetric Snow Depth product (ASD) is fully presented in Garnier et al. (2021). It is an upgraded version of the data presented in Guerreiro et al. (2016). The ASD product is provided in 500×500 EASE2 grids with a 12.5 km pixel size resolution. It is provided on a monthly basis for the six winter months.

To compute the ASD data, we use the L1b CryoSat-2 Baseline C waveforms in Pseudo Low Resolution Mode (pLRM) extracted from GOP (Geophysical Ocean Products), generated by the ESA CryoSat Ocean Processor (Bouffard et al., 2018). The Ka-band SARAL/Altika waveforms are extracted from the Centre national d'études spatiales (CNES) SGDR-T (Sensor Geophysical Data Record) official products.

3.1.2 Snow thickness algorithm

Snow depth calculations are based on the difference of penetration between the Altika Ka-band range altimeter of SARAL (assuming it is reflected at the air/snow interface) and the SIRAL Ku-band range altimeter of CryoSat-2 (assuming it is reflected at the snow/ice interface). The main assumption is that the difference between these two surface elevations is only due to the penetration of the Ku-band radar, and that the Ku-band radar penetrates fully to the snow/ice interface. The validity of this hypothesis will depend on the space and time variability of snow properties such as snow density, grain sizes, the liquid water content or the surface roughness. Since AltiKa and SIRAL operates in Low Resolution Mode (LRM) and SIRAL operates in Synthetic Aperture Radar (SAR) mode over sea ice surfaces, they have different footprints, as it is illustrated in Figure 5. The AltiKa footprint is about 8-10 km diameter while the SIRAL footprint is about 300 m in the along-track direction and as large as the antenna's cross-track footprint of about 15 km. As a consequence, the impact of the surface roughness is very different on the two signals. The use of a degraded version of the CS-2 SAR waveforms (the pLRM mode) allows to have a footprint (of about 15 km diameter) in better accordance with the LRM mode of SARAL/AltiKa waveforms, with comparable impacts of the surface roughness.

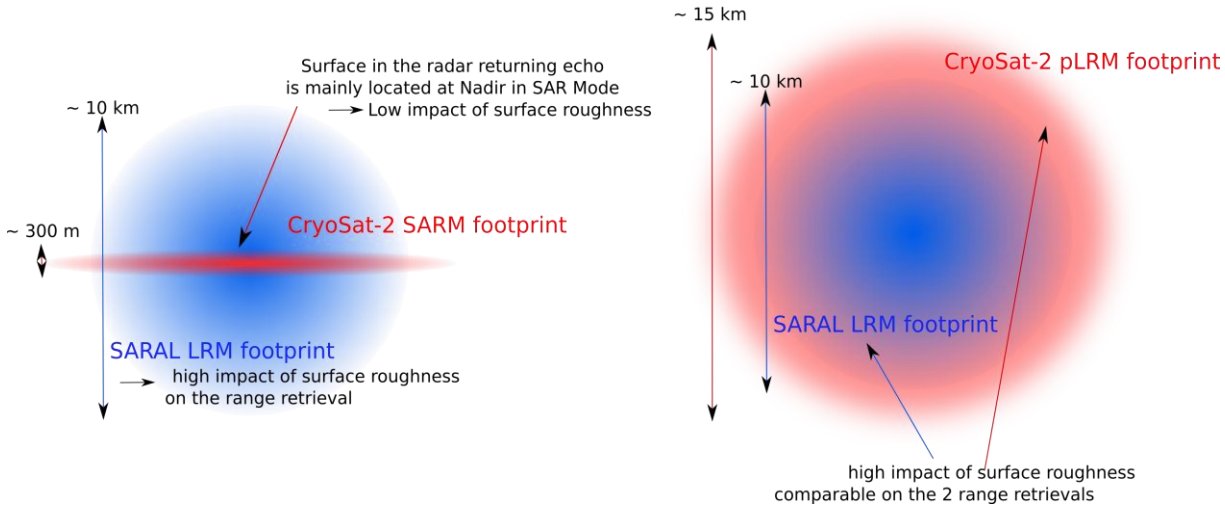

Figure 5 – Schematic representation of the footprints of SARAL and CryoSat-2 in SAR and pLRM modes. The use of the CryoSat-2 pLRM data allows to have impacts of the surface roughness on the signal in better agreement with the SARAL LRM data.

The first step to compute the ASD data consists in computing the radar freeboards of both Ku-band (in pLRM mode) and Ka-band satellite waveforms from the freeboard methodology (see Figure 5). The first step is to identify the sea ice leads and floes from the waveforms (WF) using the Pulse-Peakiness (PP) criteria. Echoes with a PP >0.3 are considered as leads and echoes with a PP < 0.1 are considered as floes. Values between 0.1 and 0.3 are considered as mixed observations and discarded. The altimeter ranges of leads and floes are calculated using the Threshold First Maximum Retracker Algorithm (TFMRA, Helm et al. (2014)) with a 50% threshold. Altimetric heights H are calculated from the altitude of the satellite, provided in the waveform products, the DTU15 Mean Sea Surface (MSS) and the relevant geophysical corrections, as described in the equation below:

-

$$tropo_{dry} + tropo_{wet} + iono + MSS + tide_{ocean} + tide$$
$$range - (\quad)$$
$$H = alt -$$

Radar freeboards fbr are then simply. fbr = $H_{floes} - H_{leads}$. Note that the choice of the geophysical corrections do not significantly impact the radar freeboard estimations.

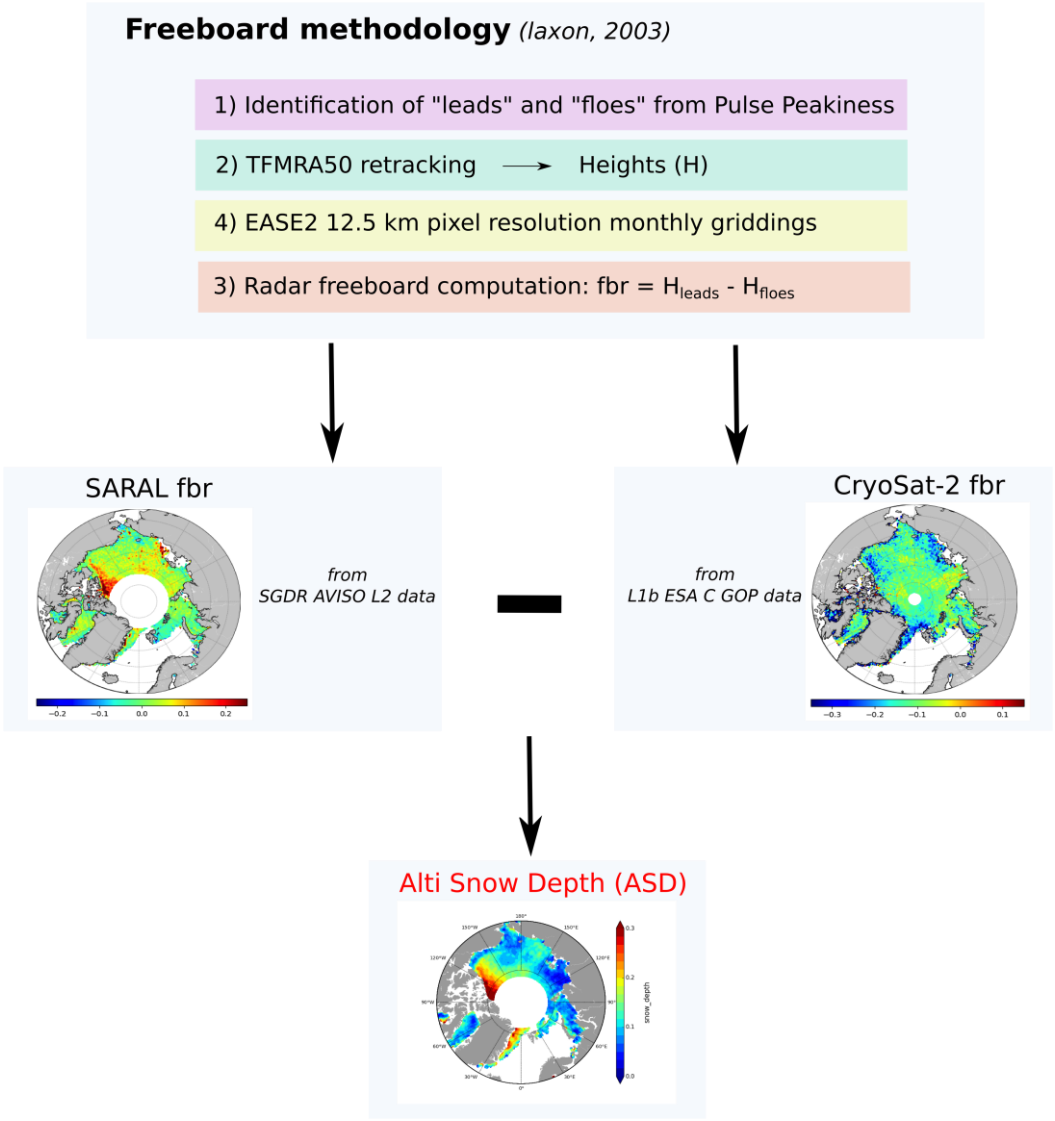

Figure 6 – Schematic representation of the methodology to compute the dual frequency Ka-Ku Alti Snow depth data.

Prior to this calculation the heights of the leads are linearly interpolated under the floes within a 25 km window. In the absence of leads in this interval, observations are discarded. Based on the EUMETSAT's Ocean and Sea Ice Satellite Application Facility (OSI SAF), observations in areas of less than 70% of sea ice are removed. Finally, a 25 km radius median smoothing is applied to the retrieved freeboards. The snow depth sd is then computed from the radar freeboards of SARAL and CryoSat-2 (fb_{Ka} and fb_{Ku}) previously gridded in 500×500 EASE2 grids with a 12.5 km pixel size resolution assuming a dominant scattering from the snow-air interface for Ka-band and from the snow-ice interface for Ku-band and considering the decrease of the Ku-band radar echo velocity as it penetrates into the snow pack (Ulaby et al., 1986, Mallett et al, 2020) following the equation below:

$$sd = (fbr_{Ka} - fbr_{Ku}) \times (1 + 0.51 \times \rho_s)^{-1.5}$$

where ρ_s is the snow density, set to 300 kg/m3.

Figure 6 presents an example of ASD snow depth estimations. We observe that the snow distribution consistently follows the dynamics of sea ice, the most characteristic of which is the export of MYI in the Beaufort gyre. It also highlights the main deviations with the W99m climatology, which tends to exhibit much thicker snow layers over sea ice. The ASD mean level of uncertainties (of about 4 cm on average with standard deviation of 1 cm) are smaller than the deviations between these two products (on average about 6 cm with standard deviation of 7 cm).

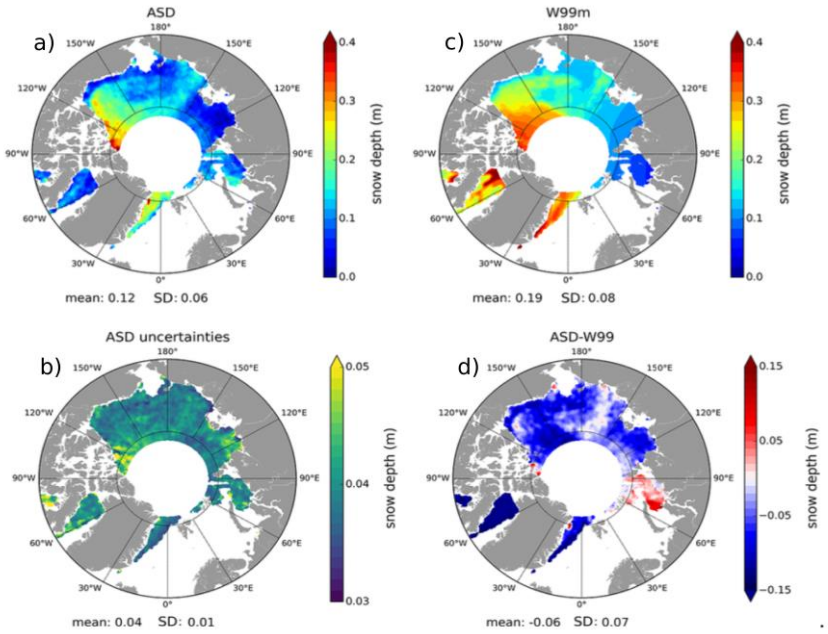

Figure 7 – Maps of the Altimetric Snow Depth (ASD) annual mean snow depth (a) and its uncertainties (b) in the Arctic for 2015. The annual mean snow depth map of the modified Warren-99 climatology (c) and its difference with the ASD product (ASD-W99m, map d) are also presented.

3.1.3 Uncertainty budget

To compute the uncertainties we assume that the errors are unbiased, uncorrelated and follow the Gaussian propagation law. The radar freeboard uncertainties δ_{fbr} are calculated from:

$$\delta_{fbr} = \sqrt{\delta^2_{H_{leads}} + \delta^2_{H_{floes}}}$$

The uncertainty of the heights of leads $\delta^2_{H_{leads}}$ is calculated along-track from the statistical variance of heights (σ_{Hleads}) and the number of observations N_{leads} and N_{floes} within a 12.5 km radius. Since sea ice topography can significantly vary, we assume that the statistical variance of floes is the same as that of the leads. The uncertainty on the radar freeboard is then:

$$\delta^2_{fbr} = \frac{\sigma_{H_{leads}}}{N_{leads}} + \frac{\sigma_{H_{floes}}}{N_{floes}}$$

Following the same assumptions and methodology, we can then deduce the formulation for the uncertainty of the snow depth δ^2_{fbr} :

$$\delta_{sd}^2 = \left(\left(\sqrt{\delta_{fb_{Ka}}^2 + \delta_{fb_{Ku}}^2} \right) \times A \right)^2 + \left((fb_{Ka} - fb_{ku}) \times B \times \delta_{\delta_s} \right)^2$$

With

$$A = (1 - 0.51\rho_s)^{-1.5} \wedge B = -1.5 \times 0.51 \times (1 + 0.51\rho_s)^{-2.5}$$

An example of the uncertainties is presented in Figure 7.

3.1.4 Latest developments

Since the dataset presented in Garnier et al, 2021, several updates have been made, that better suit with the aim of this project. In the Arctic, the ASD data are now available from March 2013 to April 2020. As already mentioned, the CS-2 pLRM baseline C is now used to compute the data for the entire period (instead of Baseline B previously). It means that the snow depth is also calculated for regions observed by CryoSat-2 in SARin mode (marginal zones). Note that the ASD products has also been computed, over the same 2013-2020 period in the Antarctic. We plan to add 2021 in the next few months.

3.2 Calibration methodology (Lawrence et al., 2018)

3.2.1 Datasets

This algorithm uses CPOM AltiKa freeboards, CPOM CryoSat-2 freeboards, CPOM Sentinel-3A/B freeboards (Lawrence et al. 2019), ATLAS/ICESat-2 L3B Daily and Monthly Gridded Sea Ice Freeboard (ATL-20), Version 1 (available from NSIDC: https://nsidc.org/data/ATL20/versions/1) , and NASA Quick Look Operation IceBridge data (also available at NSIDC: https://nsidc.org/data/NSIDC-0708/versions/1). All datasets are described in deliverable D2.2.

3.2.2 Snow thickness algorithm

This methodology builds on previous work carried out as part of the ESA-funded Arctic+ project and published in Lawrence et al. (2018). Here, in contrast to the other multi-frequency methodologies, satellite freeboards are *calibrated* with independent observations of snow and ice freeboard. It is well-understood that the extent to which radar waves interact with a snowpack is dependent on their frequency (Beaven et al. 1995). It is also well-documented that the satellite footprint size will influence the surface elevation retrieval due to (i) the impact of surface roughness on the echo waveform (Guerreiro et al. 2017; Landy et al. 2019), and (ii) greater contamination of large satellite footprints by leads, resulting in a bias towards larger, thicker sea ice floes (Tilling et al., 2019). Despite both being understood, It is difficult to separate elevation biases due to the footprint size from the physical snow penetration, without sophisticated waveform modelling strategies (e.g. Landy et al., 2019). The calibration methodology, rather than trying to separate these effects, simply corrects for both simultaneously, aligning one satellite freeboard with the air-snow interface and the other with the ice-snow interface, allowing snow depth to be estimated as the difference between the two.

The publication by Lawrence et al. (2018) applied the methodology to two sets of satellites; AltiKa and CryoSat-2 for the period 2013 to 2018, and Envisat and ICESat for their period of overlap between 2003 and 2009. Here, we extend the AltiKa vs. CryoSat-2 snow dataset to present day, altering the method slightly by including Sentintel-3A (2016-present) and Sentinel-3B (2018-present). We are

calling this combination "KuKa", not to be confused with the ground-based radar instrument. In section 4.2, we also apply the calibration method to Ku-band radar (CryoSat-2 + Sentinel-3) and laser (ICESat-2) satellites, made possible by the launch of the ICESat-2 in 2018. This pairing, in contrast to KuKa, has the advantage of extending to high latitude (88ºN), which permits a straightforward interpolation of the pole hole yielding a pan-Arctic snow-on-sea-ice dataset.

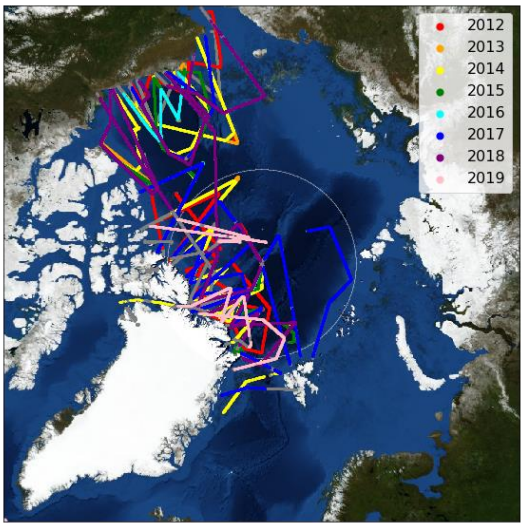

Figure 8 – NASA Operation IceBridge data utilised in the calibration method. The white circle marks 81.5º N, the latitudinal limit of the AltiKa and Sentinel-3 satellite orbits.

KuKa calibration method

Calibrating satellite freeboards requires independent observations of snow and ice freeboard. Following Lawrence et al. (2018), we use data from NASA's Operation IceBridge (OIB) airborne campaigns, which operated in the Western Arctic in the spring months of 2011 to 2019 (Figure 8). Note that while Lawrence et al. (2018) used OIB data processed by Ron Kwok at JPL, here we use the publicly available Quick Look product since the JPL dataset is not readily available. For each day of each airborne campaign, OIB snow depth and ATM laser freeboard are averaged onto a 2° longitude x 0.5° latitude grid. Grid cells with fewer than 50 measurements are removed from the analysis to reduce noise. Satellite data (Ka comprising AltiKa radar freeboards and Ku comprising CryoSat-2 and Sentinel-3 radar freeboards) for the ± 10 days surrounding the airborne campaign day are then averaged onto the same 2°x0.5° grid. Satellite Pulse Peakiness (PP), a parameter derived from the satellite waveform and a proxy for surface roughness, are also averaged to the same grid. For each day, the satellite grids are interpolated along the airborne tracks in order to compare OIB and satellite freeboard at each location where both exist. For Ka, the difference between satellite (AltiKa) radar freeboard and OIB ATM freeboard is plotted against satellite PP (Figure 9a). For Ku, the difference between OIB *radar* freeboard (calculated by subtracting OIB snow depth from ATM freeboard with a correction for the slower speed of light propagation through snow) and satellite radar freeboard is plotted as a function of PP (Figure 9b).

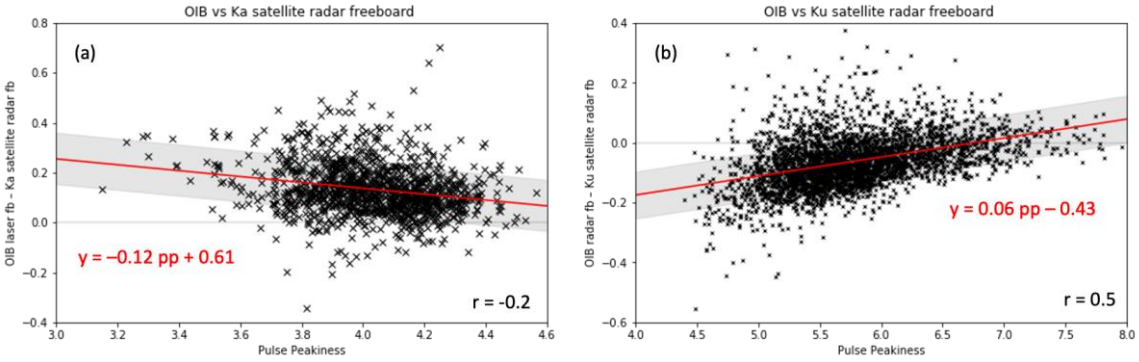

Figure 9 - Calibration functions for Ka (left) and Ku (right) satellite freeboards. For each satellite, the difference between the measured and "expected" freeboard (from OIB) is plotted as a function of Pulse Peakiness, a proxy for surface roughness. Grey shading around linear fit shows the ± 68% prediction interval, equating to 10/8cm for Ka/Ku.

By applying a linear regression to each plot, we derive a calibration function to align Ka and Ku satellite freeboards with the air-snow and snow-ice interfaces respectively. When this calibration is applied to monthly satellite freeboards, the effect is to raise Ka freeboards (Figure 10), and lower Ku (Figure 11).

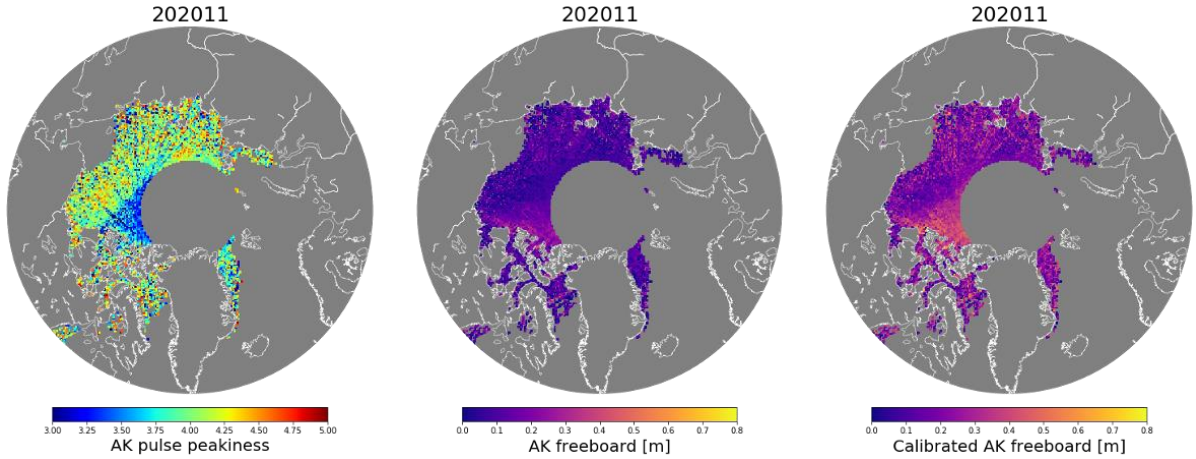

Figure 10 – Original (middle) vs. calibrated (right) Ka (AltiKa) freeboard for example month of November 2020. Freeboards are calibrated as a function of pulse peakiness (left), via the linear regression function derived above (Figure 9a).

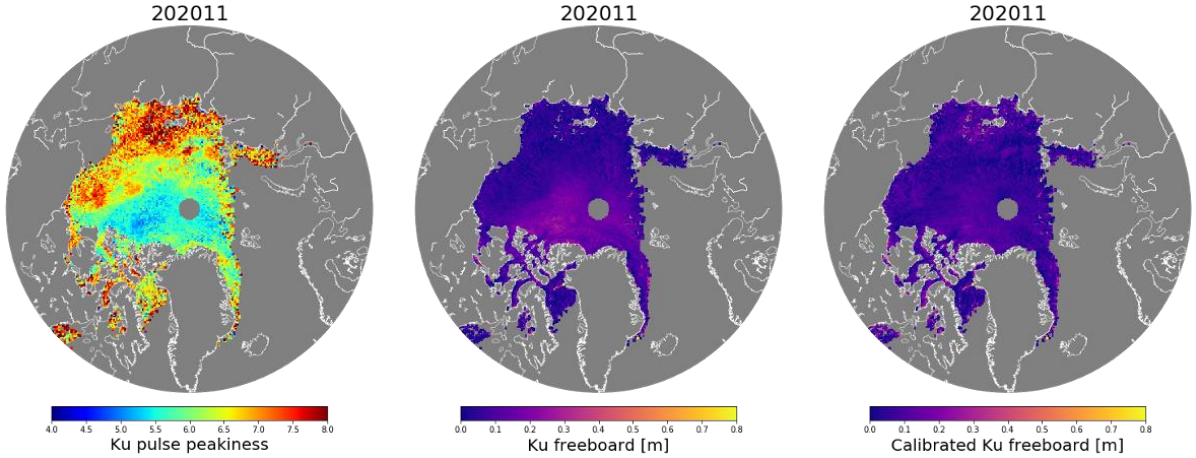

Figure 11 - Original (middle) vs. calibrated (right) Ku (CryoSat-2+Sentinel-3) freeboard for example month of November 2020. Freeboards are calibrated as a function of pulse peakiness (left), via the linear regression function derived above (Figure 9b).

Snow depth is estimated as the difference between these two calibrated freeboards, again applying a correction for the slower speed of propagation in snow such that:

$$h_s = 0.781\big((f_{Ka} + \Delta f_{Ka}) - (f_{Ku} + \Delta f_{Ku})\big)$$

Where h_s = snow depth, f_{Ka} is original Ka freeboard, Δf_{Ka} is the calibration correction applied to Ka freeboard such that $(f_{Ka} + \Delta f_{Ka}) =$ calibrated Ka freeboard, and f_{Ku} and Δf_{Ku} are the original Ku freeboard and Ku calibration correction. The value of 0.781 is derived from a ratio of $\frac{c}{c_s}$ = 1.28, as in Lawrence et al. (2018), and after (Kwok 2014). KuKa snow depth from this methodology span eight winters, from 2013-14 to 2020-21. Monthly snow depths for one winter (2019-20) are shown in (Figure 12)

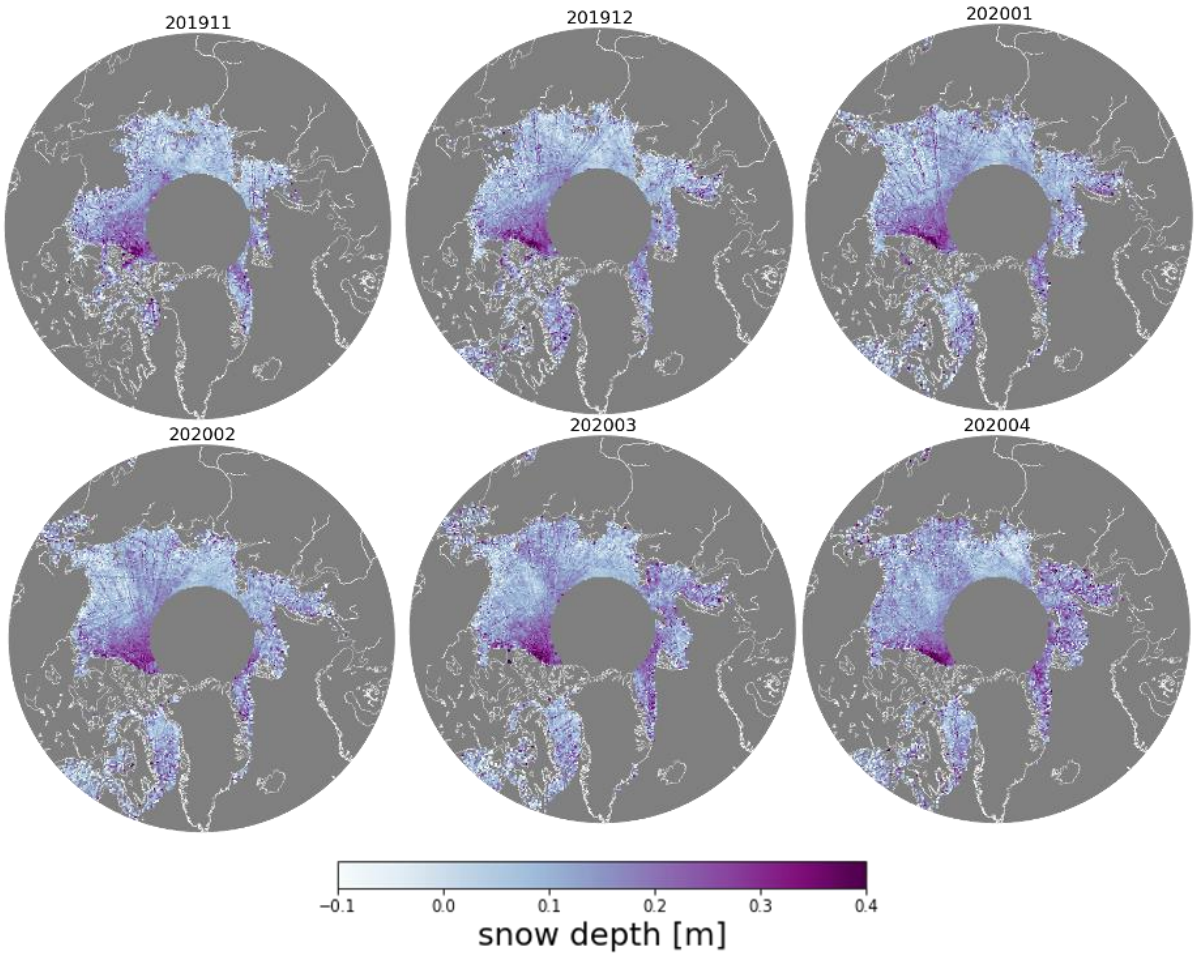

Figure 12 - Monthly snow depths for November 2019 - April 2020, derived from the KuKa calibration method.

3.2.3 Uncertainty budget

To attribute an uncertainty to KuKa snow depths, we follow the methodology in Lawrence et al. (2018). Via the calibration methodology, snow depth is expressed as:

(1)

$$h_s = 0.781\big((f_{Ka} + \Delta f_{Ka}) - (f_{Ku} + \Delta f_{Ku})\big)$$

The uncertainty on h_s is therefore given by:

$$\sigma_{h_s} = 0.781 \left(\sigma_{f_{Ka}}^2 + \sigma_{\Delta f_{Ka}}^2 + \sigma_{f_{Ku}}^2 + \sigma_{\Delta f_{Ku}}^2 + 2\sigma_{f_{Ka}\Delta f_{Ka}} + 2\sigma_{f_{Ku}\Delta f_{Ku}} - 2\sigma_{f_{Ka}f_{Ku}} - 2\sigma_{f_{Ka}\Delta f_{Ku}} - 2\sigma_{\Delta f_{Ka}f_{Ku}} - 2\sigma_{\Delta f_{Ka}\Delta f_{Ku}} \right)^{\frac{1}{2}} \quad (2)$$

Where $\sigma_{f_{Ka}}$ and $\sigma_{f_{Ku}}$ are the errors on the satellite freeboards, $\sigma_{\Delta f_{Ka}}$ and $\sigma_{\Delta f_{Ku}}$ are the errors on the calibration corrections, and the last six terms are the covariances between f_{Ka} , f_{Ku}, Δf_{Ka}, and Δf_{Ku}. As detailed in Lawrence et al. (2018) and Lawrence et al. (2019), the error on satellite radar freeboard is dominated by the sea-level interpolation which forms part of the processing routine. This error is output in the Level-2 files processed by CPOM, providing an along-track uncertainty on radar freeboard for CryoSat-2, Sentinel-3A and -B, and AltiKa. Since sea-level interpolation is performed in a 200-km along-track window, errors do not decorrelate from one along-track measurement but *do* decorrelate from one satellite pass to the next. Therefore, the uncertainty on gridded monthly freeboard reduces by $1/\sqrt{N}$, where N is the number of satellite passes per grid cell. Figure 13 shows, for an example month of 202003, how the monthly gridded uncertainty reduces as a function of the number of satellite tracks per grid cell. Note that here we are using the native 25x25km grid that the ICESat-2 ATL-20 data is provided on.

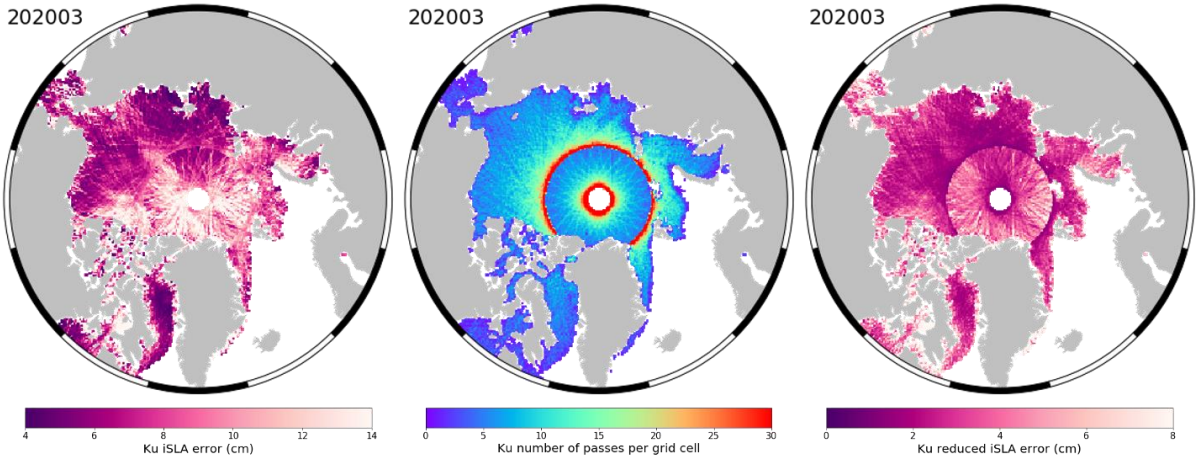

Figure 13 - Left: grid-averaged error on Ku-radar interpolated sea level anomaly (iSLA), considered a proxy for freeboard uncertainty. This along-track uncertainty, when gridded, reduces by $1/\sqrt{N}$ where N is the number of tracks per grid cell (middle). Right: The reduced iSLA error, i.e. the uncertainty on satellite radar freeboard, for an example month of 202003.

$\sigma_{\Delta f_{Ka}}$ and $\sigma_{\Delta f_{Ku}}$, the errors on the freeboard corrections, are provided by the prediction intervals on the linear regression functions shown in Figure 9, equating to 10 cm for Ka and 8 cm for Ku. Finally, the last six terms of Equation 2 express the covariances between the terms of Equation 1. For all winter (October to April) months that Ku and Ka data exist simultaneously (201303 to 202104), monthly grid-averaged f_{Ka} , f_{Ku} , Δf_{Ka} and Δf_{Ku} are appended to a file and the covariance matrix is calculated using Python's numpy.cov function. The covariances are given in Table 1. The uncertainty on KuLa snow depth for the winter of 2019-20 is shown in Figure 14, averaging to 9 cm for all months.

Covariance term	$\sigma_{f_{Ka}\Delta f_{Ka}}$	$\sigma_{f_{Ka}f_{Ku}}$	$\sigma_{f_{Ka}\Delta f_{Ku}}$	$\sigma_{\Delta f_{Ka}f_{Ku}}$	$\sigma_{\Delta f_{Ka}\Delta f_{Ku}}$	$\sigma_{f_{Ku}\Delta f_{Ku}}$
Value	0.0010	0.0041	–0.0017	0.0007	–0.0007	–0.0019

Table 1 - Covariances between satellite freeboards and freeboard corrections, required for snow depth uncertainty calculation.

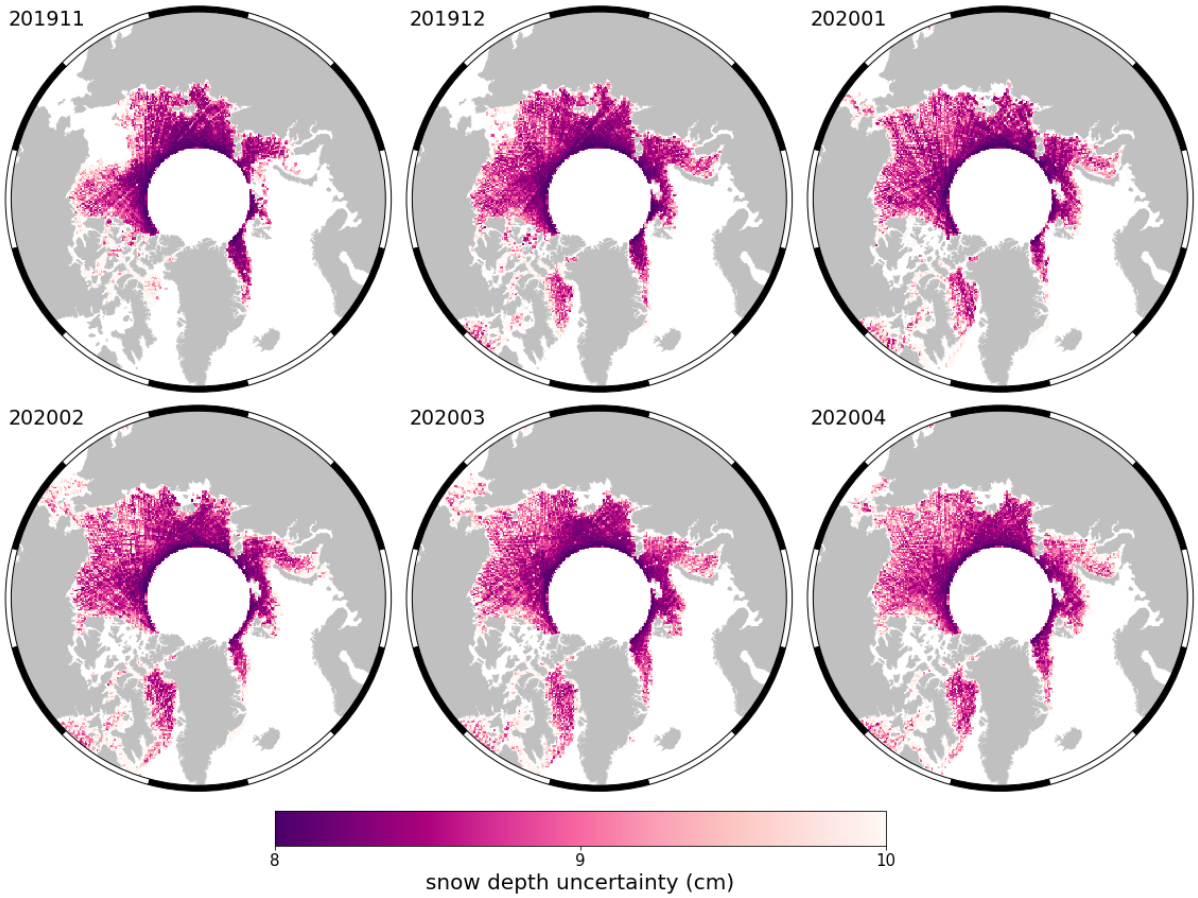

Figure 14 - Monthly snow depth uncertainty by the KuKa calibration method, for winter 2019-20.

3.2.4 Latest developments

The calibration method has been applied to satellite freeboards for the winters of 2013-14 to 2020-21. The KuKa snow depth product derived from the calibration methodology has been compared with those obtained from the bias correction and waveform modelling methodologies in Polar+ Snow WP4 and together the products have been validated against independent airborne and in situ datasets.

3.3 Waveform modelling methodology

3.3.1 Datasets

This algorithm currently uses the Baseline-D CryoSat-2 SAR- and SARIN-mode Level 1B datasets from the ESA PDS science server and the AltiKa SARAL LRM-mode Level 1B Geophysical Data Record 'sgdr_f' from AVISO Altimetry.

3.3.2 Snow thickness algorithm

The basis for the waveform modelling approach is to fit a physical model for the backscattered radar altimeter echo to observed altimeter waveforms and obtain, through the model inversion, estimates for the retracked snow-sea ice interface elevation (CryoSat-2) or air-snow interface elevation (AltiKa). Height differences between pan-Arctic monthly gridded snow-ice and air-snow elevations are corrected for the delayed travel speed of the CryoSat-2 Ku-band radar wave through snow to produce estimates for the pan-Arctic snow depth. (Note this method has not yet been through peer review).

The fundamental assumption of the method is that forward model solutions for the CryoSat-2 Ku-band SAR echo or AltiKa Ka-band LRM echo adequately represent the height of the snow-ice or air-snow interface, respectively, based on the physical mechanisms scattering or reflecting the radar wave at each frequency. Here we take the simple approach to model both Ku-band and Ka-band radar returns from a single scattering surface, assumed to represent the snow-ice and air-snow interfaces, respectively. Several studies have called this assumption into question. For instance, volume scattering from snow grains or brine and surface scattering from the air-snow interface and/or interstitial interfaces within the snowpack (e.g., ice lenses, layers) may attenuate the Ku-band radar wave sufficiently to elevate the primary Ku-band radar scattering horizon above the snow-ice interface (Willatt et al., 2011; Ricker et al., 2015; Nandan et al., 2017; King et al., 2018). Equally, variations in snow grain size and density, brine content, and the radar-scale roughness of the snow surface may depress the primary Ka-band radar scattering horizon below the air-snow interface (Larue et al., 2021). These processes are unlikely to occur consistently in different regions of the Arctic and periods of the sea ice growth and snow accumulation season (Armitage and Ridout, 2015). In the case our fundamental assumption of a single scattering interface is invalidated and/or the model inadequately reproduces the true scattering response of the radar wave, we will obtain a bias in the retracked elevation.

In the case of a single scattering surface the radar altimeter echo model is parameterized by four terms: A, the scaled waveform amplitude, t_0, the tracking point of the mean radar scattering surface (or 'epoch'), σ, the surface topography root-mean square height, and s_{rms}, the small-scale roughness. This is assuming that variations in the radar antenna parameters (e.g., satellite altitude, velocity, off-nadir pointing angle) have a negligible impact on the shape of the sea ice waveform return and can be ignored.

The alternative option would be to forward model the full combination of possible surface and volume scattering mechanisms (e.g., see Figure 15d), then invert for many more free terms over a much larger multi-dimensional parameter space. However, the inversion for a single scattering surface is already ill posed, with four parameters to be solved from one observation (the power waveform). Solving for more parameters without further data increases the likelihood of inversion errors, such as finding local parameter minima in the waveform fitting scheme.

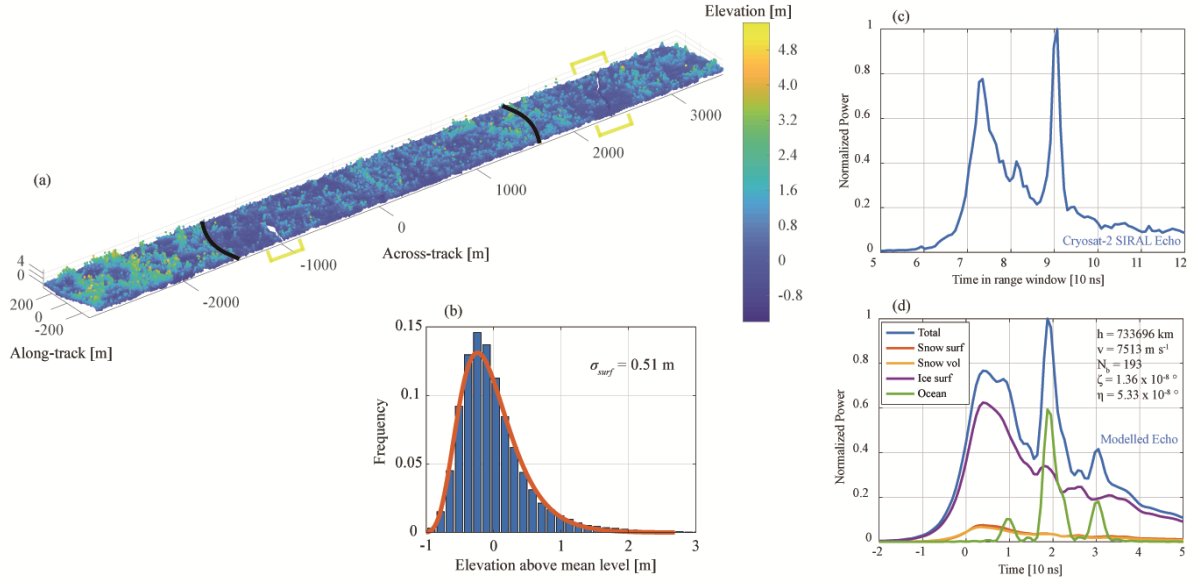

Figure 15 – Application of the Facet-Based Echo Model (FBEM) to forward simulate a CryoSat-2 return from sea ice topography based on Operation IceBridge (OIB) airborne laser scanner observations from the Lincoln Sea. (a) Snow surface elevation model from the OIB Airborne Topographic Mapper (ATM) showing the CryoSat-2 pulse limited footprint in black and the locations of two leads crossing the footprint in yellow. (b) Snow surface height distribution and best fitting Lognormal model. (c) Actual observed CryoSat-2 waveform from the footprint. (d) Simulated total CryoSat-2 waveform (blue) and estimated contributions from air-snow interface, snow volume scattering, snow-ice interface, and ocean lead reflections, with inset CryoSat-2 sensing parameters. From Landy et al. (2019).

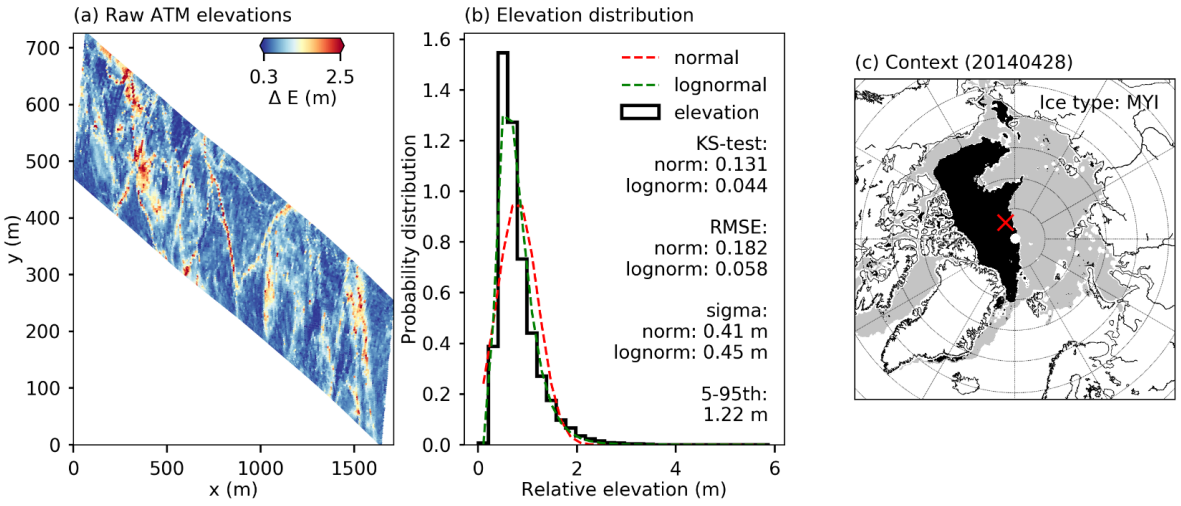

Figure 16 – Comparison of Gaussian (normal) and Lognormal statistical models fit to the observed snow surface height distribution on sea ice from OIB ATM data at the scale of the CryoSat-2 footprint. (a) Snow surface elevation from the ATM over multi-year sea ice in the Central Arctic. (b) Observed elevation distribution from the ATM with best fitting normal and Lognormal models, including statistics from Kolmogorov–Smirnov tests, RMSE, and standard deviations (roughness) of the two model fits. (c) Data source location. From Landy et al. (2020).

We use the Facet-Based Echo Model (FBEM) which simulates the radar altimeter echo as the integral of the power backscattered from a tetrahedral mesh representing the sea ice surface topography (Landy et al., 2019). The FBEM is available as an open-source MATLAB code from here https://github.com/jclandy/FBEM. The scattering mechanisms are characterized for each facet of the

mesh. Backscatter from the air-snow or snow-ice interface is obtained from the sum of the scattered and reflected components, simulated with the Integral Equation Model (IEM; Fung, 1994) and physical optics approximation (Fung and Eom, 1983), respectively. The balance between scattering and reflection depends on the radar frequency and mm-cm scale 'radar' roughness of the surface (Landy et al., 2020). The FBEM can also simulate snow volume scattering and reflections from off-nadir leads, as shown in the example in Figure 15d. However, both of these scattering mechanisms are neglected for our simplified 'single surface' waveform modelling scheme here.

The air-snow and snow-ice interfaces are characterized by a Lognormal probability density function of the height distribution e.g. (Figure 15b), following Landy et al. (2020). This is based on observations from the NASA Operation IceBridge airborne laser scanner and Ku-band radar that show both interfaces are more accurately characterized by a Lognormal model than a Gaussian model, at the ~kilometre scale of a satellite altimeter footprint. This is the case for both first-year ice (FYI) and multi-year sea ice (MYI) (Figure 16).

A lookup table of Ku-band SAR altimeter echoes were simulated from FBEM for sea ice surfaces with Lognormal height PDF, σ ranging from 0 to 1 m, and s_{rms} ranging from 0 to 6 mm, as described in Landy et al. (2020). Radar antenna parameters are characterized for the CryoSat-2 SIRAL instrument (Landy et al., 2019). Examples for the modelled SAR echoes with fixed s_{rms} of 2 mm but varying σ are shown in Figure 17a. The parameter s_{rms} controls the incidence angle dependence of the radar backscattering coefficient and mainly effects the trailing edge of the waveform. The parameter σ controls the roughness of the large-scale sea ice topography and principally effects the width of the waveform leading edge (Figure 17a). Zero time on Figure 17a represents the radar tracking point t_0 and is crossed at a different amplitude of the waveform leading edge power depending on σ. This implies that the relative retracking amplitude should decrease as the large-scale roughness of the snow-ice interface increases, from around 95% for σ=0 to 65% for σ=0.5 m.

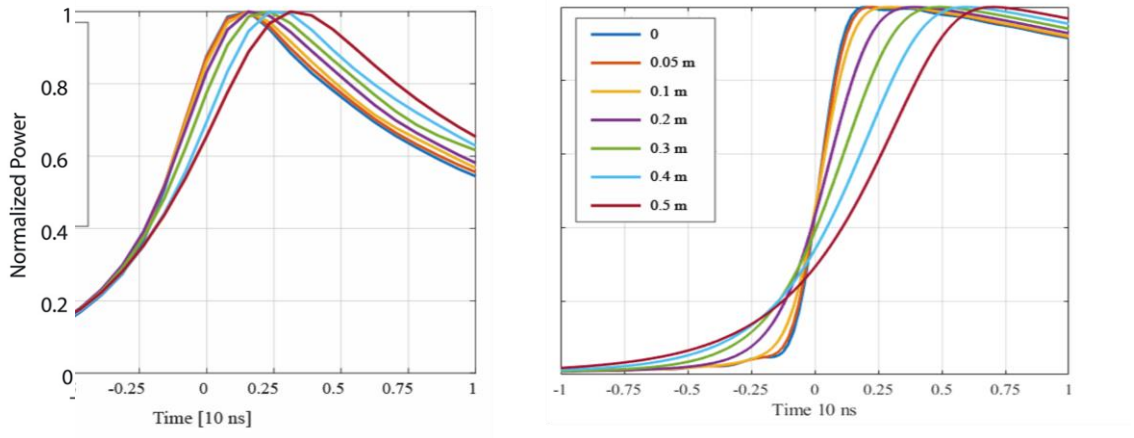

Figure 17 – Radar echo simulations for a single scattering interface (snow or sea ice), with a Lognormal roughness height distribution and different roughness standard deviations, in (Left) Ku-band SAR-mode with radar sensing parameters from CryoSat-2 SIRAL and (Right) Ka-band LRM-mode with radar sensing parameters from AltiKa SARAL.

A lookup table of Ka-band LRM altimeter echoes were also simulated from FBEM for sea ice surfaces with Lognormal height PDF, σ ranging from 0 to 1 m, and s_{rms} ranging from 0 to 6 mm. Radar antenna parameters are characterized for the AltiKa SARAL instrument, based on https://directory.eoportal.org/web/eoportal/satellite-missions/s/saral. Examples for the modelled LRM echoes with fixed s_{rms} of 2 mm but varying σ are shown in Figure 17b. The roughness of the large-scale sea ice topography σ again impacts the width of the waveform leading edge. The radar

tracking point t_0 is also again crossed at a different amplitude of the waveform leading edge power depending on σ (Figure 17b). This implies that the relative retracking amplitude for LRM waveforms should also decrease as the large-scale roughness of the air-snow interface increases, from around 50% for σ=0 to 25% for σ=0.5 m.

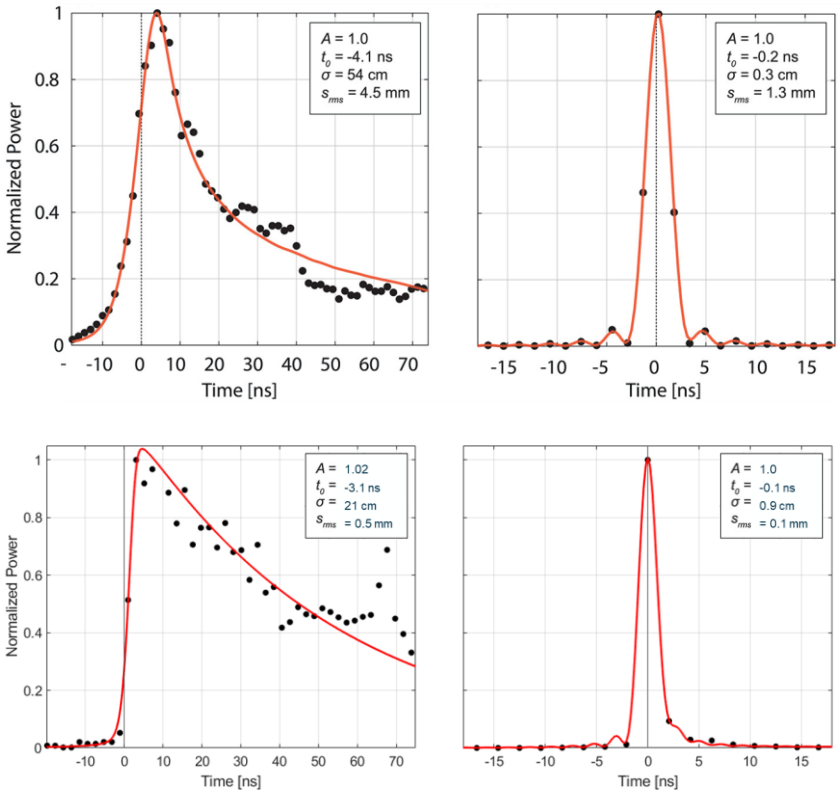

Figure 18 – Best fitting model echoes to observed radar waveforms from (Top Row) CryoSat-2 SAR-mode and (Bottom Row) AltiKa LRM-mode. The left-hand plots show model fits to characteristic diffuse-type waveforms returned from a rough sea ice or snow surface. The right-hand plots show model fits to characteristic specular-type waveforms returned from smooth ocean lead surfaces. The zero time marks the 'epoch' or radar retracking point, i.e. the mean level of the scattering surface. The free parameters optimized during waveform fitting are inset: A = normalized waveform amplitude, t_0 = time difference of epoch to the time at waveform peak power, σ = large scale surface roughness, s_rms = mm-cm radar-scale surface roughness. Adapted from Landy et al. (2020).

We use a least-squares fitting procedure to optimize the functional form of the modelled sea ice echo to observed CryoSat-2 or AltiKa waveforms. The fitting routine is based on the bounded trust region reflective algorithm (implemented through the *MATLAB* function *lsqnonlin*) to minimize the difference between the model fit and each observed power waveform, as described in Landy et al. (2020). At the end of the fitting procedure, we obtain best fit estimates for the four free parameters: A, t_0, σ, and s_{rms}. Examples for the best-fitting modelled echoes to sea ice surfaces and leads, for both CryoSat-2 and AltiKa waveforms, are shown in Figure 18 along with their associated parameters. It is evident that the large-scale topography rms σ and small-scale roughness s_{rms} are both larger for the sea surfaces than for leads. It is also notable that zero padding applied to CryoSat-2 SAR waveforms prior to the range FFT, which enhances the range resolution, provides a better constraint on the elevation of leads than can be obtained from the lower range-resolution AltiKa LRM waveforms (Figure 18).

A low-pass filter is applied to the along-track height profile to remove residual sea surface topography with a horizontal wavelength greater than 200 km. The sea surface height anomaly (SSHA) is then obtained at ice-covered locations from a linear interpolation between lead elevations, along the orbit

of the satellite, as described in Landy et al. (2020). All sea ice observations >200 km from their nearest lead are discarded. Along-track radar freeboards are calculated from the elevation difference between sea ice floes and the interpolated SSHA. Finally, the radar freeboards for both CryoSat-2 and AltiKa are gridded at a resolution of 50 km on the same EASE2 pan-Arctic projection using a simple binned mean algorithm. The gridded CryoSat-2, AltiKa SARAL radar freeboards and corresponding ICESat-2 laser freeboards are shown for December 2019 in Figure 19. The CryoSat-2 freeboards are clearly smaller than either than AltiKa or ICESat-2 freeboards, and all three datasets show relatively thicker freeboards over the MYI than over the FYI zone. It is evident, however, that the AltiKa radar freeboards show more local spatial variability than either CryoSat-2 or ICESat-2 freeboards, which is potentially attributable to noise.

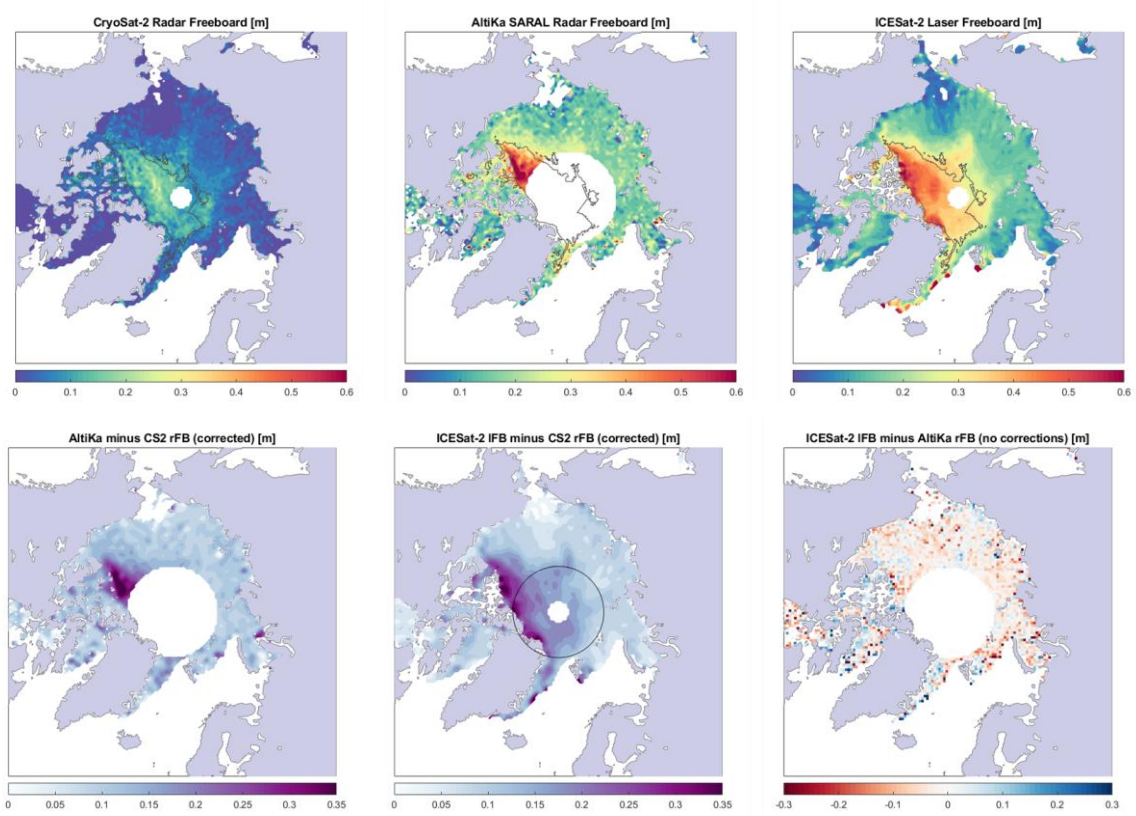

Figure 19 – Example of the CryoSat-2 and AltiKa radar freeboards obtained from physical-model waveform fitting in December 2019, with comparison to ICESat-2 laser freeboards. On the bottom row are two estimates for the snow depth obtained from a simple difference between KuKa freeboards and KuLa freeboards (see below), corrected for the delayed Ku-band wavespeed through the snow volume. A map of the difference between the two derived snow depth estimates is shown in the bottom left.

We assume that the CryoSat-2 radar freeboards represent the elevation of the snow-ice interface, but this is not corrected for the delayed Ku-band wave propagation velocity through the snowpack. To derive estimates for the snow depth from the height difference in gridded radar freeboards, we multiply the height difference by 0.781, which corresponds to the ratio of radar wave velocities between free space and snow with density 350 kg m-3 (Lawrence et al., 2018). The derived snow depth maps for corrected AltiKa minus CryoSat-2 radar freeboards (KuKa), and for corrected ICESat-2 laser freeboards minus CryoSat-2 radar freeboards (KuLa), are also shown in Figure 19. There are some clear similarities between the two products, including thicker derived snow depths over MYI north of Canada and in Fram Strait, than over FYI in the surrounding Arctic seas. However, the KuLa maps show

more regional variability in snow depth than the KuKa maps, especially where mean snow depth is estimated to be very thin (<10 cm) around the edges of the sea ice pack in the KuLa product. The height differences between AltiKa radar freeboards and ICESat-2 laser freeboards show no clear regional patterns, but the AltiKa freeboards are slightly higher (~2 cm) on average than the ICESat-2 freeboards (Figure 21). This bias is reversed by April 2020, with AltiKa freeboards slightly lower (~5 cm) on average than the ICESat-2 freeboards (data not shown).

The seasonal cycle in KuKa derived snow depth for the 2019-20 sea ice growth season demonstrates that snow depth on MYI always exceeds that on FYI (Figure 20). There is a minor increase in snow depth recorded over FYI and MYI between November and February, although the mean depth over MYI shows a decrease between February and April. Overall, the pan-Arctic mean snow depth increases from 12 to 17 cm between November and April.

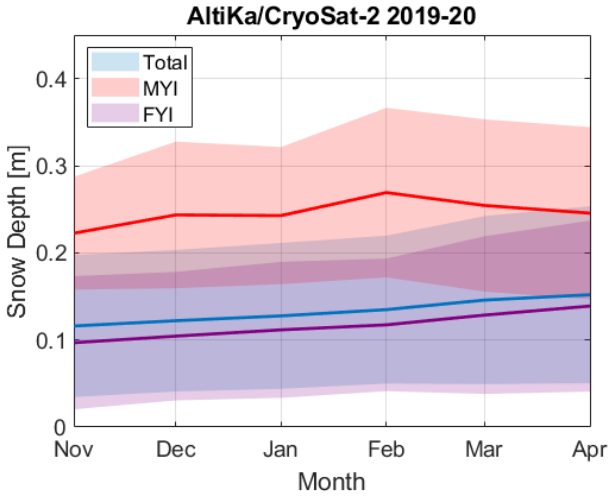

Figure 20 – Time series for the seasonal change in snow depth obtained from physical model-based KuKa radar freeboards over the 2019-20 sea ice growth/snow accumulation season. The envelopes represent +/- one standard deviation around the mean snow depth.

3.3.3 Uncertainty budget

There is no formal uncertainty budget for the waveform fitting method, but we have examined noise and potential biases in KuKa derived snow depths by comparing to KuLa derived snow depths. The distributions of pan-Arctic gridded radar and laser freeboard from CryoSat-2, AltiKa and ICESat-2 for December 2019 are shown in Figure 21a. It is notable that the CryoSat-2 radar freeboard distribution is much narrower with a primary mode at 5 cm and a portion of grid cells having freeboard around zero or slightly negative. MYI freeboards are evident as a small secondary mode of the CryoSat-2 distribution between 10 and 20 cm. The AltiKa radar freeboard and ICESat-2 laser freeboard distributions appear very similar, with a primary mode around 15-16 cm; however, the ICESat-2 distribution contains a secondary mode of thinner freeboards around 4-10 cm (highlighted by the grey circle) that is not evident in the AltiKa distribution. The trailing edges of the AltiKa and ICESat-2 distributions have a similar shape, representing thicker MYI. Derived KuKa and KuLa snow depth distributions in Figure 21b have almost the same mode, although the KuKa depths overestimate KuLa by a few centimetres and the distribution is wider. The mean freeboard ratio between AltiKa and ICESat-2 (Figure 21c) is around 1.05. If we assume the KuLa snow depths are more realistic, then it is

likely the wider KuKa snow depth distribution is caused by higher noise in the AltiKa freeboards than in CryoSat-2/ICESat-2 freeboards (Figure 19).

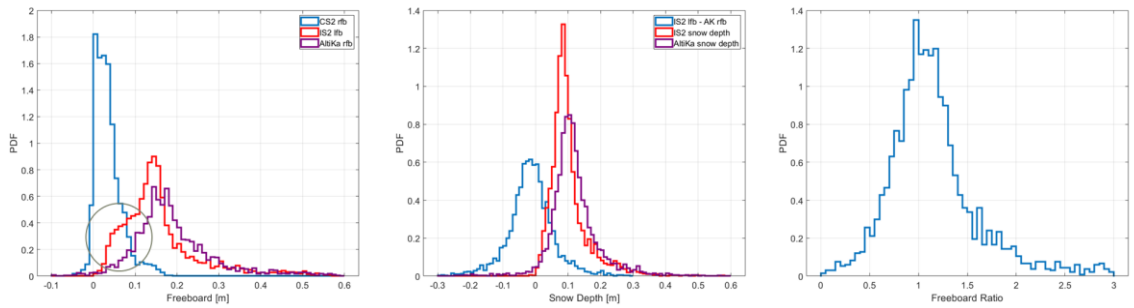

Figure 21 – Comparison of the gridded radar freeboards obtained from physical model waveform fitting applied to CryoSat-2 and AltiKa to laser freeboards obtained from ICESat-2 in December 2019. (Left) Freeboard distributions. (Middle) Derived snow depth distributions and the distribution of gridded differences between AltiKa and ICESat-2. (Right) The AltiKa freeboards plotted as a ratio of the ICESat-2 freeboards. (Note that distributions only cover the coinciding region of observations between the three sensors south of 81.5N).

It is challenging to identify the source or sources of bias between the KuKa and KuLa snow depths. They could be caused by (i) the principal scattering horizon of the Ku- or Ka-band radar wave not aligning with the snow-ice or air-snow interface, respectively, owing to radar penetration or surface roughness related effects. (ii) The ICESat-2 laser penetrating into the snowpack (ref). (iii) Our model for the radar altimeter not adequately simulating the true backscattered radar response in SAR or LRM mode. (iv) Our model assumption of a single scattering surface not being valid, owing to strong contributions from snow volume scattering or reflections from interfaces within the snowpack. (v) Inaccurate waveform classification erroneously removing or including sea ice floe or lead elevation measurements in the CryoSat-2 or AltiKa freeboard products. Any one or combination of these effects could produce a mismatch between the AltiKa and ICESat-2 freeboards, that we are assuming both measure the height of the air-snow interface.

We have investigated the relationship between sea ice surface roughness and systematic offsets between radar freeboards from AltiKa and laser freeboards from ICESat-2 in Figure 22. Here we compare the footprint-scale surface roughness parameter σ obtained from the AltiKa waveform inversion scheme to the mean (and one standard deviation) of the gridded AltiKa freeboards minus ICESat-2 freeboards. This relationship is characterized from all altimeter observations collected between November 2019 and April 2020. The AltiKa-derived roughness σ in January 2020 is generally higher over MYI (20-40 cm) than over FYI (<15 cm), with the exception of regions experiencing strong sea ice dynamics such as around the New Siberian Islands (Figure 22a). In areas of lower surface roughness (<12 cm) the AltiKa and ICESat-2 freeboards are almost equivalent, with a standard deviation in the gridded differences of around 10 cm. However, as the roughness increases the AltiKa freeboards increasingly and systematically overestimate the freeboards from ICESat-2 (Figure 22b). This may highlight the impacts of roughness on the significance of different radar scattering mechanisms at Ka-band (e.g., Larue et al., 2021). Alternatively, it may highlight deficiencies in the accuracy of our model for Ka-band LRM echoes, or in the steps taken after waveform retracking to filter valid observations, such as the waveform classification. These open questions will be examined in the near future.

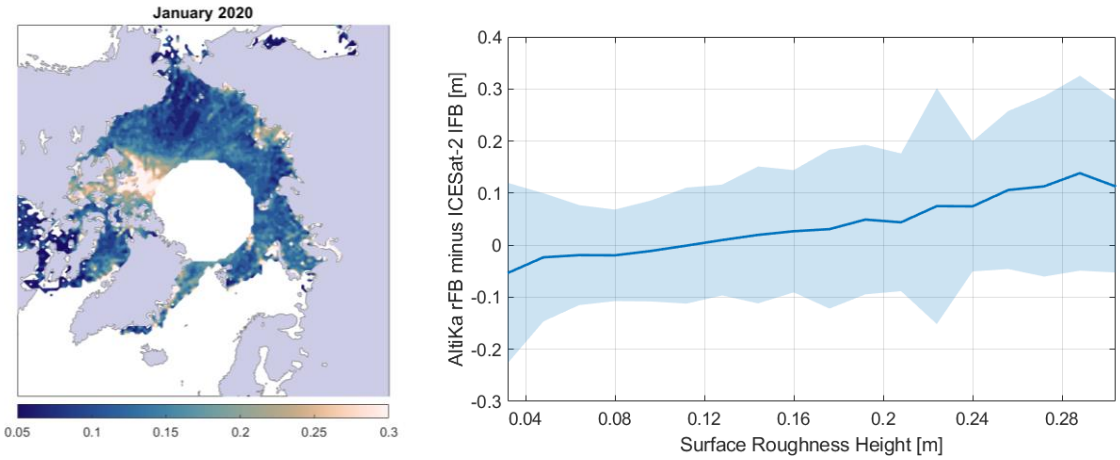

Figure 22 – The relationship between AltiKa surface roughness (left) and the apparent difference between Ka-band and laser freeboards from AltiKa and ICESat-2, respectively (right). The relationship is characterized from all measurements between Nov 2019 and Apr 2020. The systematic bias between AltiKa and ICESat-2 increases as a function of the derived Ka-band radar surface scattering roughness.

3.3.4 Latest developments

The waveform modelling method for KuKa has been applied to the sea ice growth seasons October-April in 2018-19, 2019-20 and 2020-21. The KuKa snow depth product derived from waveform modelling has been compared with those obtained from the bias correction and calibration methodologies in Polar+ Snow WP4 and together the products have been validated against independent airborne and in situ datasets.

4 Prototype Ku Radar – Laser (KuLa) snow thickness retrieval algorithms

4.1 LEGOS methodology

4.1.1 Datasets

The LaKu product is provided in 712 x 712 EASE2 grids with a 12.5 km pixel size resolution. It is provided on a monthly basis from October to April from 2018 to 2021 over Arctic.

To compute the LaKu data, we use the CryoSat-2 Baseline-D&E (the waveforms are the same) in SAR and SARin processed with SAMOSA+ retracker by GPOD and with TFMRA50 by LEGOS. The freeboards are computed using the LEGOS sea-ice processor. The Laser data from ICESat-2 are extracted from NSIDC (https://nsidc.org/data/). We use the ATL10 product version 4.

CryoSat-2 carries a synthetic interferometric altimeter Ku-band instrument which operates in 3 modes:

Low Resolution Mode (LRM): it consists of conventional pulse-width limited altimetry with a footprint of 7 km radius

Synthetic Aperture Radar (SAR): the mode used over sea ice. It enables to reduce the footprint size along the track to about 300 m.

SAR interferometric: this mode operates at the margin of ice caps

We used the SAR and SARIn mode to compute the freeboard. The footprint size is indicated on Figure *23*.

ICESat-2 has on board a space-based lidar, the Advanced Topographic Laser Altimeter System (ATLAS). ATLAS measures the travel time of laser photons from the satellite to Earth and back. ATLAS emits visible laser pulses at 532 nm wavelength. ATLAS generates six beams arranged in three pairs in order to better determine the surface's slope and provide more ground coverage. Each beam pair is 3.3 km apart across the beam track, and each beam in a pair is separated by 2.5 km along the beam track. The footprint radius is about 17 m. Figure *23* summarizes the footprint details for both missions.

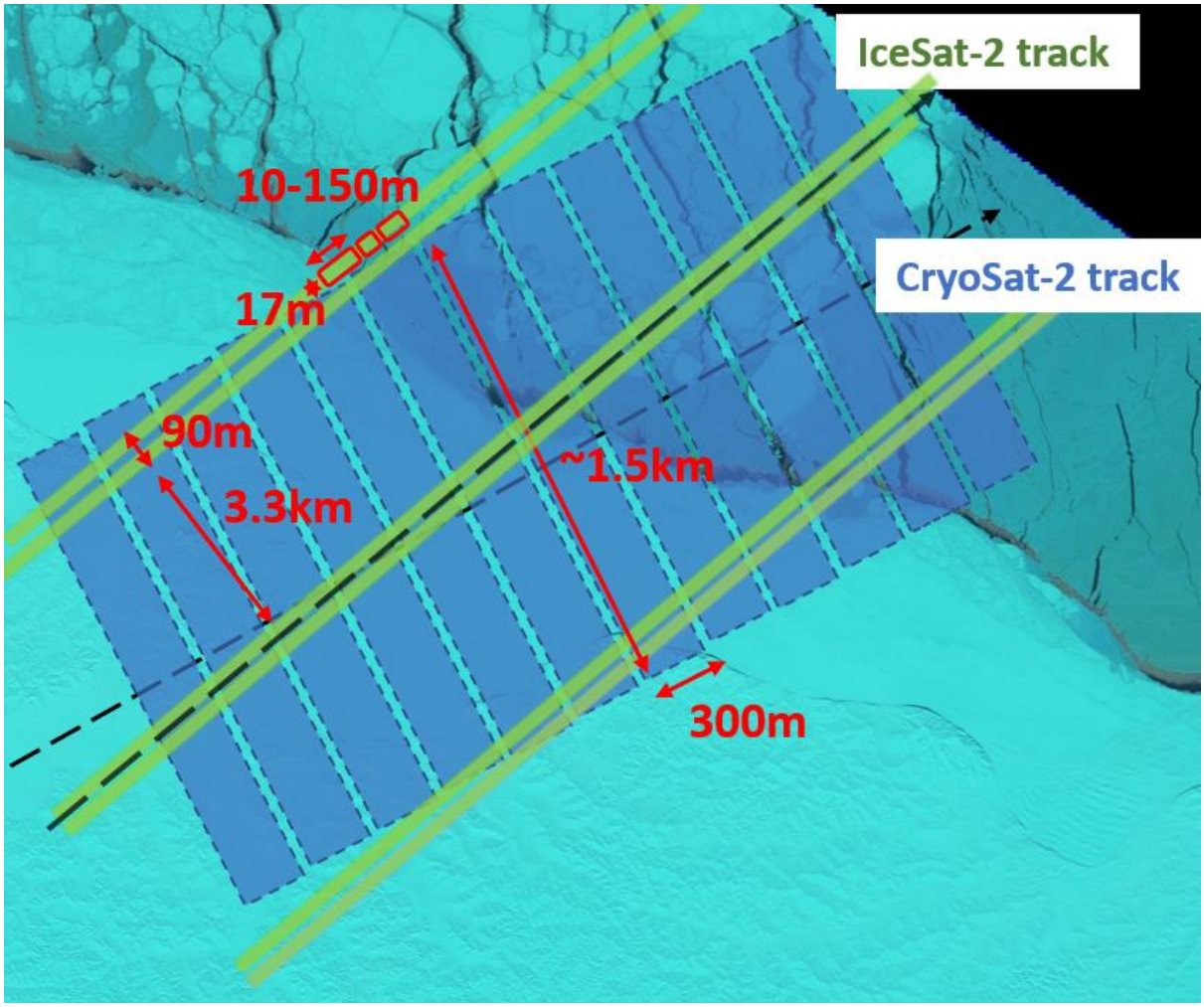

Figure *23 - Footprint details for CryoSat-2 and ICESat-2 missions*

4.1.2 Snow thickness algorithm

The computation of snow depth is based on the difference of penetration between laser altimetry of ICESat-2 – which does not penetrate snow – and the Ku-band radar altimetry of CryoSat-2 – which is assumed to be reflected not far from the snow/ice interface. As explained in 3.1.2 the main assumption is that the difference between these two surface elevations is only due to the penetration of the Ku-band radar, and that the Ku-band radar penetrates fully to the snow/ice interface. We know nevertheless that it is not always the case in particular when the snow is salty or wet. Some studies are on-going to try to apply a correction on the penetration over FYI.

The $LaKu_{LEGOS}$ product is available for 2 different freeboards with the SAMOSA+ and TFMRA50 retracker. TFMRA50 is an empirical retracker, the methodology is explained in 3.1.2. SAMOSA+ (Dinardo et al., 2018) is a physical retracker, available for sea ice surfaces, which uses a physical model to fit the waveforms.

The data are then gridded per month with a 12.5 km pixel size resolution.

The snow depth is then computed from the difference between the gridded freeboard products, by applying a snow correction to account for the speed propagation reduction of Ku in snow on CryoSat-2 data. We use Ulaby et al., 1986 equations:

$$FB_{ice} = FB_{Ku} + \left(\frac{c}{c_{snow}} - 1\right) SD = FB_{laser} - SD \quad (1)$$

$$\frac{c}{c_{snow}} = (1 + 0.00051\rho_{snow})^{1.5} \quad (2)$$

$$SD = (1 + 0.0051\rho_{snow})^{-1,5}(FB_{laser} - FB_{Ku}) \quad (3)$$

where ρ_{snow} is the snow density and is equal to 290 kg/m^3. An example is shown in Figure 24.

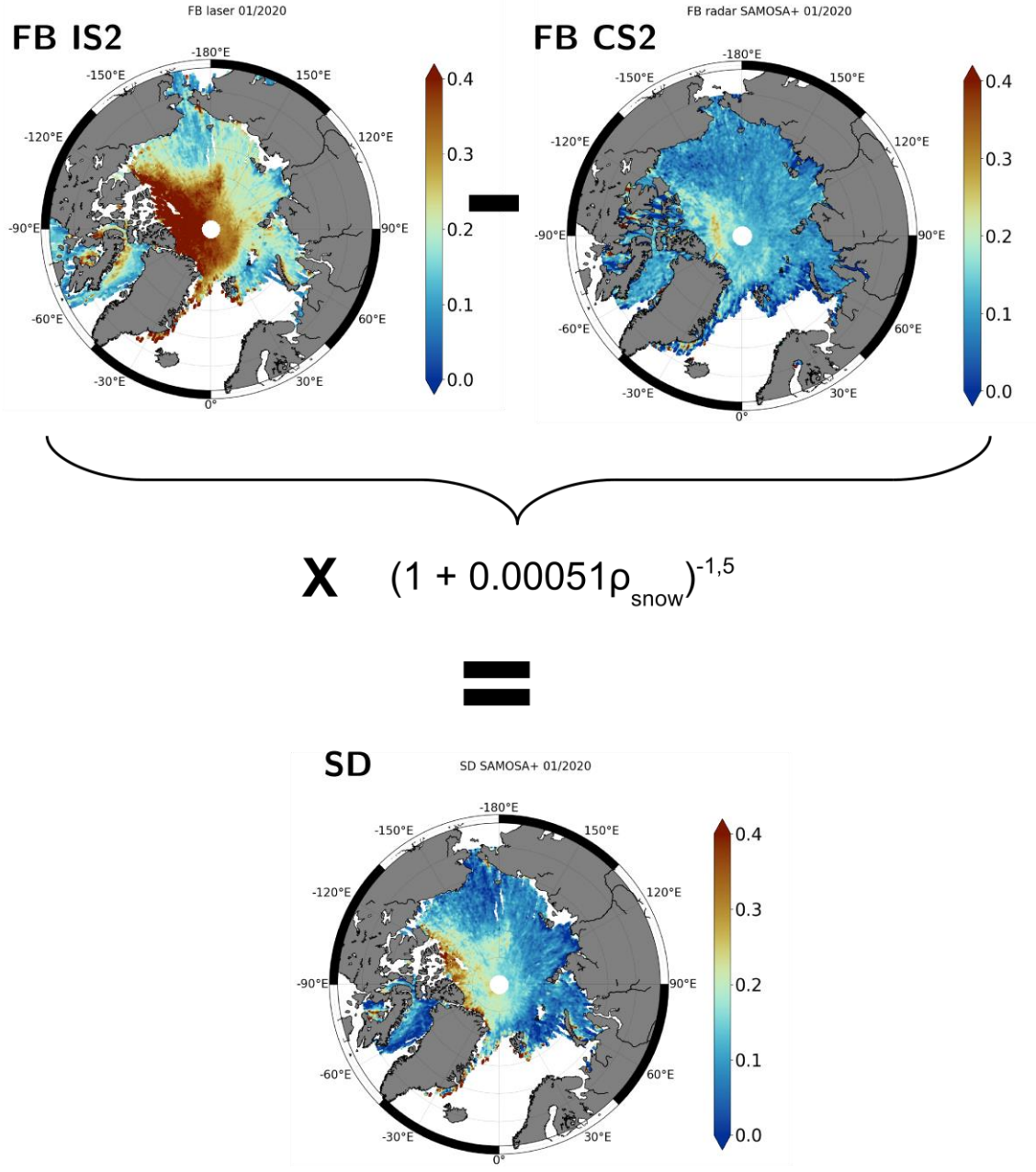

Figure 24 - Maps of a) CryoSat-2 Freeboard using the SAMOSA+ retracker ; b) ICESat-2 Freeboard and c) resulting snow over January 2021

4.1.3 Uncertainty budget

As for the other products there is no uncertainty budget for this LaKu snow depth. However, the differences between the 2 freeboards computed with CS2, one with TFMRA50 and one with SAMOSA+, can provide an idea of the uncertainties.

These differences are represented on Figure 25 for January 2020.

Figure 25 shows that the differences can be quite important especially near the Canadian Archipelago. Laforge et al., 2020 have studied the impact of these 2 retrackers on the FB retrieval and shown that it depends on the surface roughness.

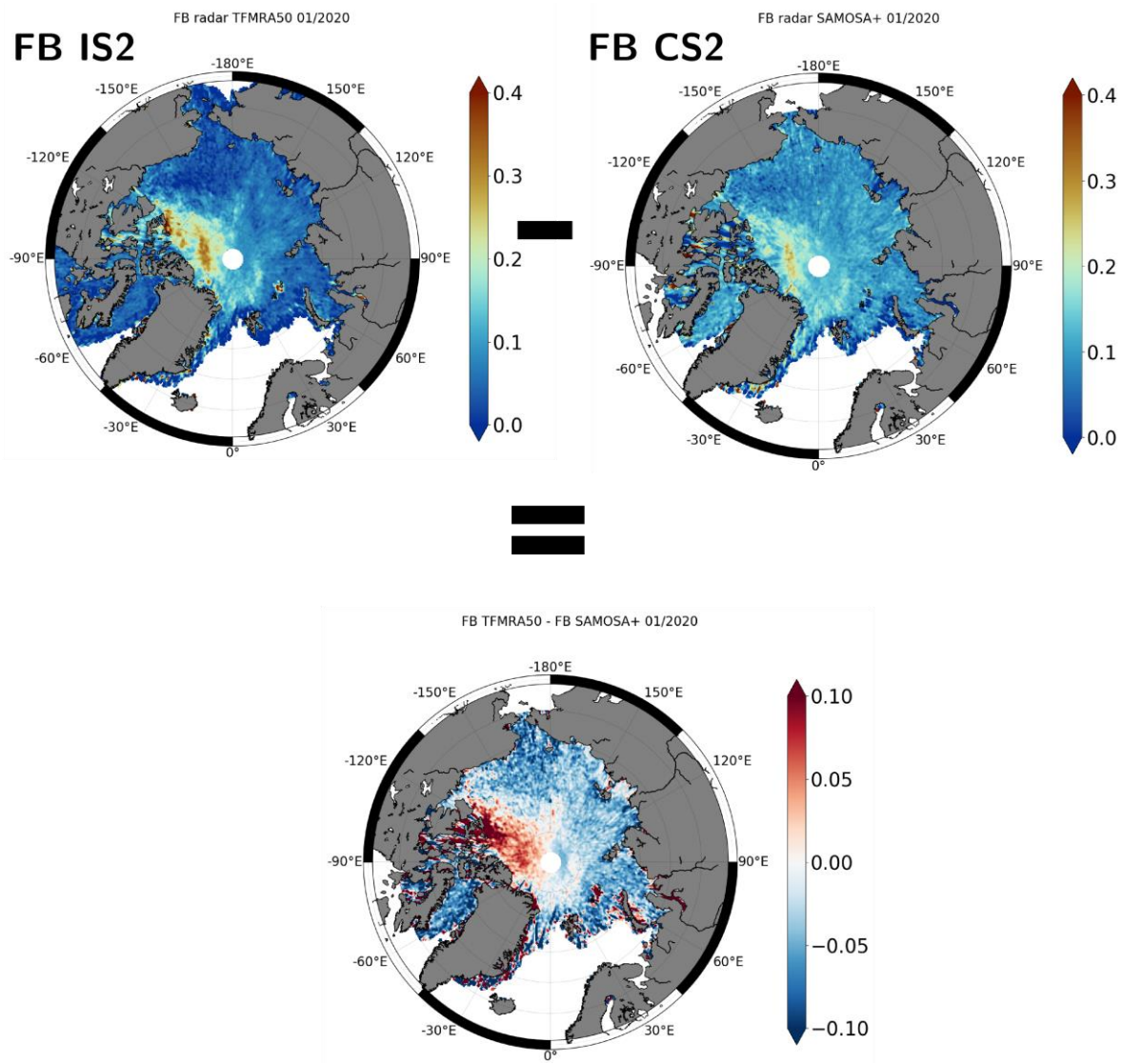

Figure 25 - Maps of CryoSat-2 freeboard using a) TMFRA50 and b) SAMOSA+. c) Difference between the freeboards.

4.1.4 Latest developments

Currently the dataset is being extended to the winter 2021-2022.

4.2 Calibration methodology (Lawrence et al., 2018)

4.2.1 Datasets

This algorithm uses CPOM CryoSat-2 freeboards, CPOM Sentinel-3A/B freeboards (Lawrence et al. 2019), ATLAS/ICESat-2 L3B Daily and Monthly Gridded Sea Ice Freeboard (ATL-20), Version 1 (available from NSIDC: https://nsidc.org/data/ATL20/versions/1) , and NASA Quick Look Operation IceBridge data (also available at NSIDC: https://nsidc.org/data/NSIDC-0708/versions/1). All datasets are described in deliverable D2.2.

4.2.2 Snow thickness algorithm

KuLa calibration method

The methodology for snow depth retrieval using Ku radar and laser (ICESat-2) freeboards, "KuLa", begins with the same calibration of Ku freeboards using OIB, i.e. the same linear function (Figure 9b) is used to calibrate Ku freeboard as a function of satellite PP. Since ICESat-2 is a laser altimeter and assumed not to penetrate the snow pack, we assume that ICESat-2 freeboard provides a measure of the true snow freeboard without the need for calibration (Lawrence et al. (2018) made this same assumption for ICESat). Here we use the ATL-20 ICESat-2 monthly gridded freeboard product, provided by NSIDC on a 25km square grid in Polar Stereographic projection.

Since ICESat-2 freeboards are not calibrated, snow depth by this methodology is given by:

$$h_s = 0.781\left(f_{La} - (f_{Ku} + \Delta f_{Ku})\right)$$

Where h_s = snow depth, f_{La} is the gridded ICESat-2 freeboard, f_{Ku} is original Ka freeboard, Δf_{Ku} is the calibration correction applied to Ku freeboard such that $(f_{Ku} + \Delta f_{Ku}) =$ calibrated Ka freeboard. Monthly snow depths for one winter (2019-20) are shown in (Figure 26). Note that there is currently a >1 year latency with the ATL-20 product, therefore we can only currently derive snow depths for two winters (2018-19 and 2019-20) with the KuLa calibration technique at present.

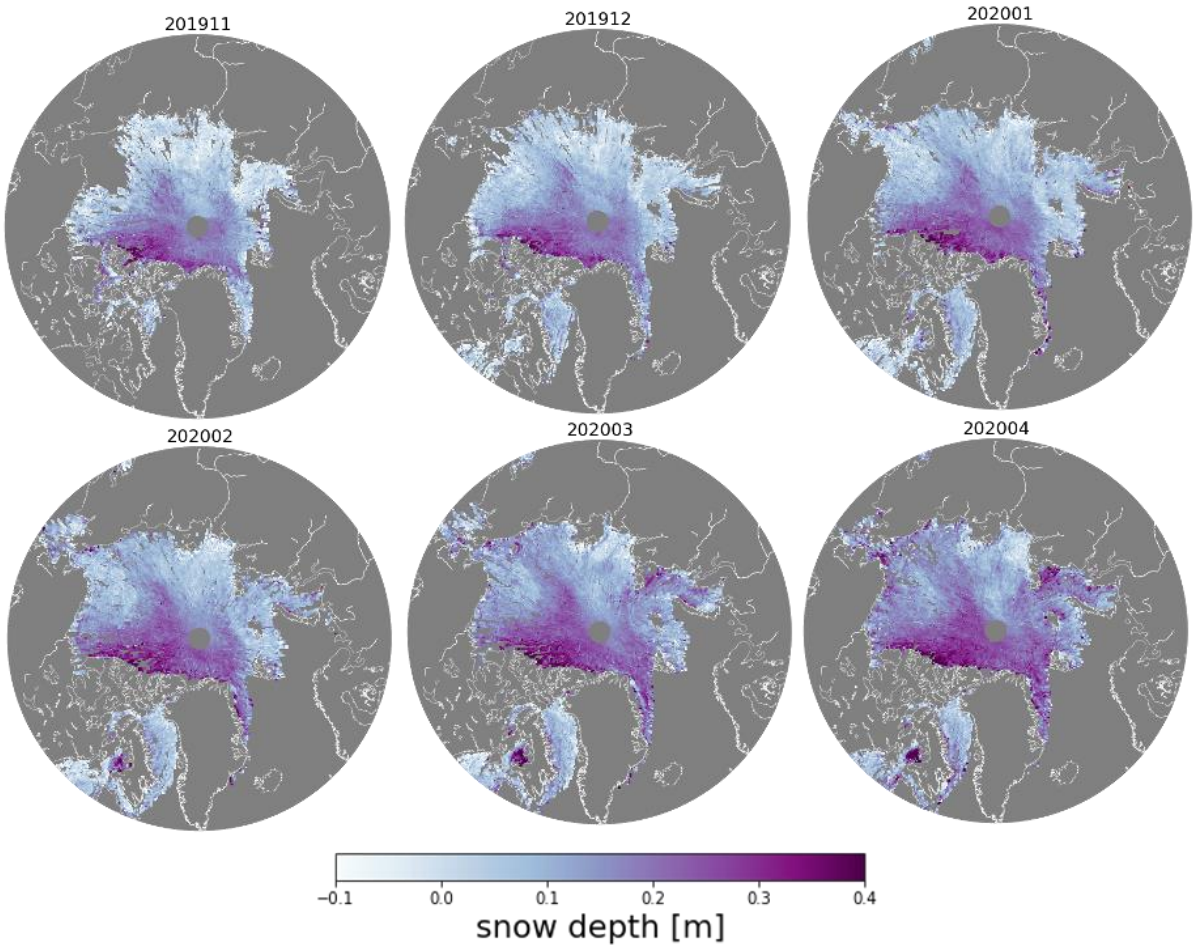

Figure 26 - Monthly snow depths for November 2019 - April 2020, derived from the KuLa calibration method

4.2.3 Uncertainty budget

Via the calibration methodology, KuLa snow depth is expressed as:

$$h_s = 0.781\left(f_{La} - \left(f_{Ku} + \Delta f_{Ku}\right)\right) \tag{3}$$

By propagation of uncertainty, the error on h_s is therefore given by:

$$\begin{gathered} -2\sigma_{f_{La}f_{Ku}} - 2\sigma_{f_{La}\Delta f_{Ku}} \\ \sigma_{f_{La}}^2 + \sigma_{f_{Ku}}^2 + \sigma_{\Delta f_{Ku}}^2 + 2\sigma_{f_{Ku}\Delta f_{Ku}} \end{gathered} \tag{4}$$

$$\sigma_{h_s} = 0.781$$

Where $\sigma_{f_{La}}$ and $\sigma_{f_{Ku}}$ are the errors on the satellite freeboards, $\sigma_{\Delta f_{Ku}}$ is the error on the Ku calibration correction, and the last three terms are the covariances between f_{La} , f_{Ku} and Δf_{Ku}. At present, monthly gridded ICESat-2 freeboards (ATL-20) are not distributed with an uncertainty estimate. Therefore, rather than using the propagation of uncertainty equation with $\sigma_{f_{La}}$ = 0, we use the previously-calculated error on KuKa snow depth (9 cm) as an upper-bound estimate for KuLa snow

depth uncertainty. This is justified, since the calibrated Ku-freeboard used in each of the products is the same and the uncertainty of ICESat-2 freeboard (though not known) is expected to be smaller than that of calibrated AltiKa freeboard.

4.2.4 Latest developments

The calibration method has been applied to satellite freeboards for the winters of 2018-19 and 2019-20. Note the current >1-year latency with the availability of ATL-20 freeboards limits the timeliness of snow depths by this methodology. The KuLa snow depth product derived from the calibration methodology has been compared with those obtained from the bias correction and waveform modelling methodologies in Polar+ Snow WP4 and together the products have been validated against independent airborne and in situ datasets.

4.3 Waveform modelling methodology

4.3.1 Datasets

This algorithm currently uses the Baseline-D CryoSat-2 SAR- and SARIN-mode Level 1B datasets from the ESA PDS science server and the ICESat-2 ATL20 gridded sea ice laser freeboard product Version 3 available from NSIDC.

4.3.2 Snow thickness algorithm

The KuLa snow depth methodology through waveform modelling has a similar basis to the KuKa waveform modelling methodology. The CryoSat-2 radar freeboards are processed in an identical manner to Section 3.3.3, i.e., by fitting a physical model for the Ku-band SAR echo to retrack CryoSat-2 L1B waveform observations, estimating the local sea surface height anomaly, and calculating freeboards along track. Here the gridded CryoSat-2 radar freeboards at 50 km resolution are used for deriving KuLa snow depths.

ICESat-2 laser freeboards are assumed to provide a good measurement of the elevation of the air-snow interface, with little penetration of the green laser into snow. This assumption has been validated by comparing the ICESat-2 laser freeboards against OIB laser scanner data (Kwok et al., 2019). We resample the ICESat-2 laser freeboard product from ATL20 to the same 50-km grid as the CryoSat-2 radar freeboards (Figure 19). It is evident that the ICESat-2 freeboards typically show a broader distribution of thickness, across the Arctic, than the CryoSat-2 radar freeboards (Figure 20).

We assume that the CryoSat-2 radar freeboards from waveform modelling represent the elevation of the snow-ice interface, but this is not corrected for the delayed Ku-band wave propagation velocity through the snowpack. To derive estimates for the snow depth from the height difference in gridded freeboards, we multiply the height difference between ICESat-2 and CryoSat-2 freeboards by 0.781, following the same approach as the waveform modelling method for KuKa. The derived snow depth maps for corrected ICESat-2 laser freeboards minus CryoSat-2 radar freeboards (KuLa) are shown for the 2019-2020 winter sea ice growth season in Figure 27. These maps show the accumulation of snow over winter, with the average snow depth on Arctic sea ice increasing from around 10 cm in November 2019 to around 18 cm by April 2020 (Figure 28). As a first check on the consistency between CryoSat-2 and ICESat-2 freeboards, the grey contour on the November 2019 snow depth map in Figure 27 highlights snow depths below 5 cm. There are large regions of 1000s square km at the sea ice pack margins where snow depths are <5 cm, in regions of new ice formation where we expect little snow to have accumulated. This supports the idea that CryoSat-2 radar freeboards and ICESat-2 laser

freeboards are measuring approximately the same elevation for new thin ice where snow depth is low or absent, and there is not an artificial systematic bias between the freeboards.

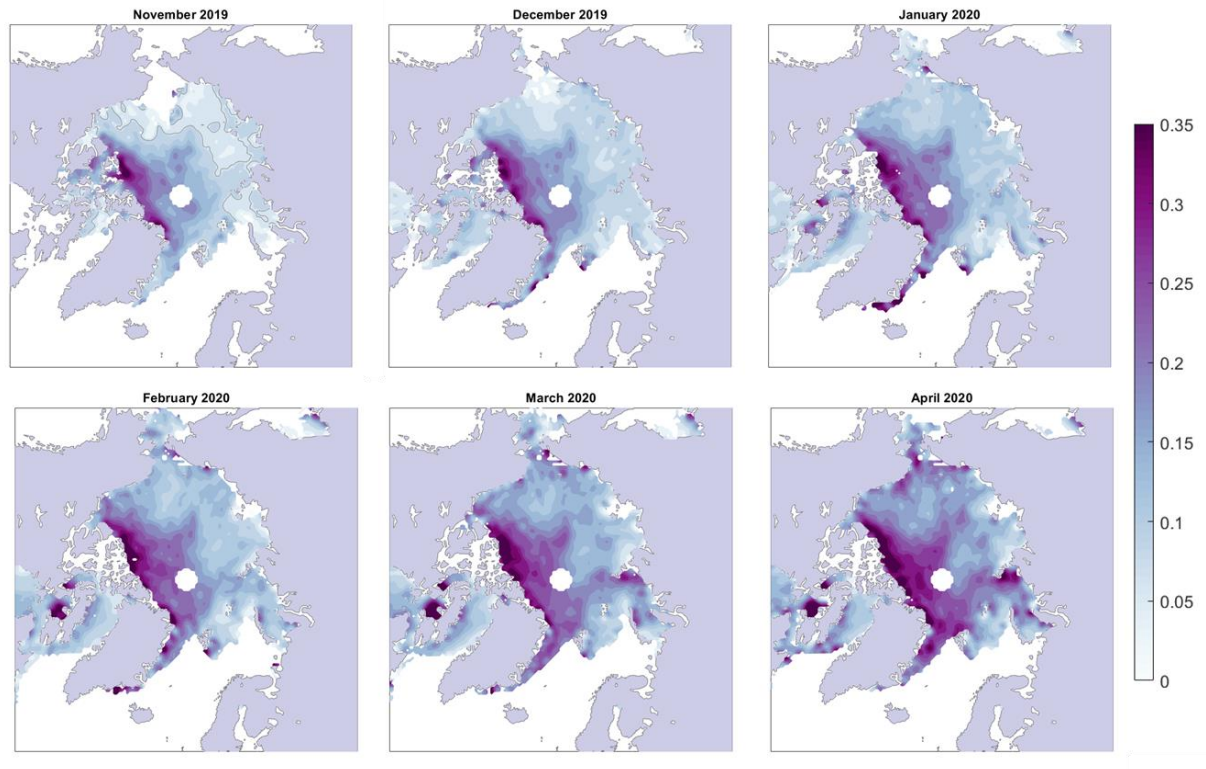

Figure 27 – Snow depth derived from the KuLa algorithm over 2019-20 applying physical waveform fitting to CryoSat-2 and using the ICESat-2 data from NSIDC ATL20 Version 3. The grey contour in the November map marks all regions where the CryoSat-2 and ICESat-2 freeboards are within 5 cm of each other.

Estimated Kula snow depths are larger over multi-year ice (around 15-38 cm) than over first-year ice (around 2-25 cm) across the snow accumulations season (Figure 28). The accumulation of snow on MYI is slower than on FYI, however, at a mean accumulation rate of around 1.5 cm/month on MYI versus around 2 cm/month on FYI.

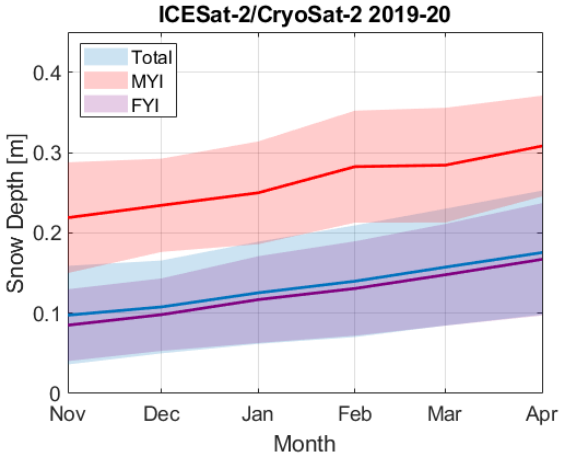

Figure 28 – Time series for the seasonal change in snow depth obtained from physical model-based CryoSat-2 Ku-band radar freeboards and ICESat-2 laser freeboards over the 2019-20 sea ice growth/snow accumulation season. The envelopes represent +/- one standard deviation around the mean snow depth.

4.3.3 Uncertainty budget

There is no formal uncertainty budget yet for the KuLa snow depth estimates based on waveform fitting. However, close-to-coinciding measurements from CryoSat-2 and ICESat-2 along *Cryo2Ice* profiles have been used to intercompare along-track KuLa snow depths obtained from different data processing methods for Nov-Dec 2020 (Figure 29). This work has been completed by Antoine Laforge (SERCO). The laser freeboards from ICESat-2 come from the NSIDC ATL10 product and are fixed, but the CryoSat-2 radar freeboards along *Cryo2Ice* profiles vary with different methods for processing CryoSat-2 data (including waveform retracking, classification, and calculation of freeboard). CryoSat-2 radar freeboards used in this intercomparison include those from the waveform fitting method (UoB) and the calibration method (CPOM). ESA Baseline D geophysical data record (ESA_BD_GDR) and the LEGOS application of the SAMOSA+ retracker (LEGOS_SAM) and TFMRA 50% retracker (LEGOS_T50) are also shown, but note the LEGOS freeboards are not the same as those used for the bias correction method outlined here (which utilized CryoSat-2 pseudo-LRM mode observations).

It is evident from Figure 29a that the distribution of freeboards from CryoSat-2 can vary significantly depending on the processing methodology. The different processing options represent a variability on the final KuLa derived snow depth (here 'Δfb_{La-Ku}') of around 5 cm. The patterns of the KuLa snow depths obtained from the mean freeboard differences along *Cryo2Ice* profiles (Figure 29b) are similar to those shown in Figure 27, with thicker snow depths corresponding to regions of MYI.

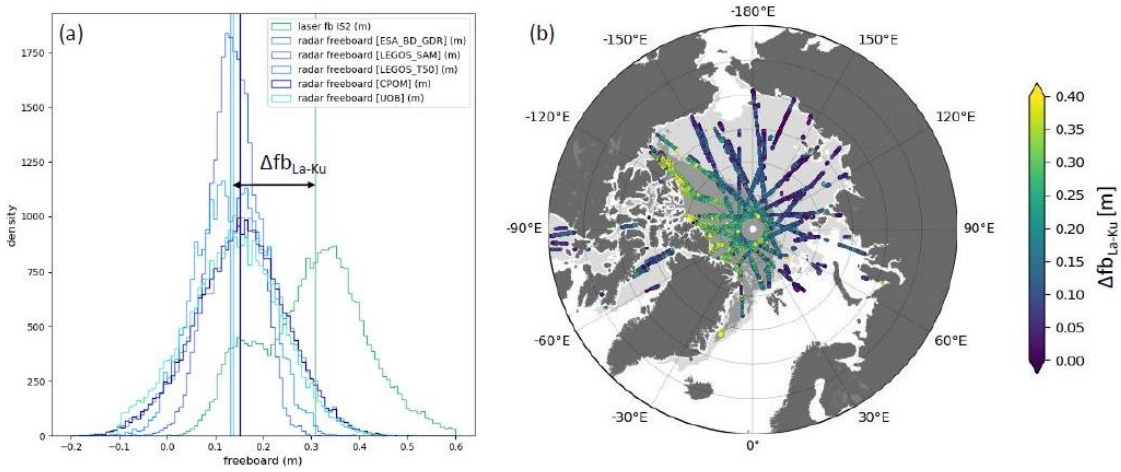

Figure 29 – (a) The distribution of Ku-band radar freeboard from multiple processing algorithms: ESA Baseline-D (ESA_BD_GDR), the LEGOS using SAMOSA+ (LEGOS_SAM) and TFMRA50 retrackers (LEGOS_T50), CPOM, and the University of Bristol LARM retracker (UOB) next to the laser freeboard from ICESat-2 ATL10 product (IS2) for collocated tracks from the period between 1st Nov 2020 and 31st Dec 2020. (b) shows the geographical distribution of the mean freeboard differences for the same period. Courtesy of Antoine Laforge.

4.3.4 Latest developments

The waveform modelling method for KuLa has been applied to the sea ice growth seasons October-April in 2018-19,2019-20, and 2020-21. The KuLa snow depth product derived from waveform modelling have been compared with those obtained from the calibration methodology in Polar+ Snow WP4 and together the products have been validated against independent airborne and in situ datasets.

5 Summary

This Algorithm Theoretical Baseline Document has summarised six different algorithms for retrieving snow depth on sea ice from multi-mission multi-frequency satellite altimetry. This includes three algorithms applied to AltiKa SARAL and CryoSat-2 SIRAL observations to retrieve "KuKa" snow depths and three algorithms applied to ICESat-2 ATLAS and CryoSat-2 SIRAL observations to retrieve "KuLa" snow depths. The document has provided detailed justification for the scientific basis and processing steps used for each algorithm.

Data products generated from the five different algorithms have then been intercompared with each other and with independent in situ and airborne snow depth observations, as well as snow depth products from modelling/reanalysis-based systems, in WP4 (D3.2 PVR; D4.1 Experimental dataset). WP4 describes the procedure to identify an optimal pan-Arctic snow depth product for Polar+ Theme 1 'Snow on sea ice' as a best performing single or ensemble merged dataset.

Direct intercomparisons between ICESat-2 and CryoSat-2 have been investigated along *Cryo2Ice* orbits (Figure 30), by Alice Charet (ESA/SERCO).

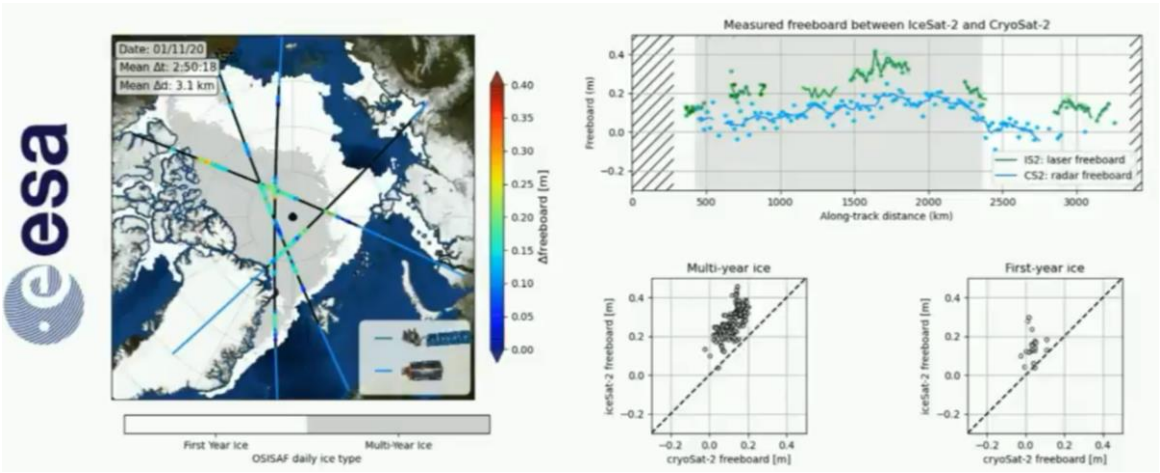

Figure 30 – Direct intercomparison between radar freeboards from CryoSat-2 and laser freeboards from ICESat-2 along aligned *Cryo2Ice* orbits, with the differences in freeboard between sensors illustrating the snow cover over multi-year and first-year ice. Courtesy of Antoine Laforge.

References

Armitage, T. & Ridout, A., 2015. Arctic sea ice freeboard from AltiKa and comparison with CryoSat-2 and Operation IceBridge. Geophys. Res. Lett., 42(16), pp. 6724-6731.

Beaven, S. G., G. L. Lockhart, S. P. Gogineni, A. R. Hosseinmostafa, K. Jezek, A. J. Gow, D. K. Perovich, A. K. Fung, and S. Tjuatja. 1995. "Radar Backscatter from Bare and Snow-Covered Saline Ice Sheets." International Journal of Remote Sensing 16 (5): 851–76.

Fung, A. & Eom, H., 1983. Coherent scattering of a spherical wave from an irregular surface. IEEE Trans. Geosci. Rem. Sens., 31(1), pp. 68-72.

Fung, A. K., 1994. Microwave Scattering and Emission Models and Their Applications. s.l.:Artech House, Inc..

Garnier, F., Fleury, S., Garric, G., Bouffard, J., Tsamados, M., Laforge, A., Bocquet, M., Fredensborg Hansen, R.M. and Remy, F., 2021. Advances in altimetric snow depth estimates using bi-frequency SARAL and CryoSat-2 Ka–Ku measurements. The Cryosphere, 15(12), pp.5483-5512.

Guerreiro, Kevin, Sara Fleury, Elena Zakharova, Alexei Kouraev, Frédérique Rémy, and Philippe Maisongrande. 2017. "Comparison of CryoSat-2 and ENVISAT Freeboard Height over Arctic Sea Ice: Toward an Improved Envisat Freeboard Height Retrieval." The Cryosphere 11: 2059–73. https://doi.org/10.5194/tc-11-2059-2017.

King, J. et al., 2018. Comparison of Freeboard Retrieval and Ice Thickness Calculation From ALS, ASIRAS, and CryoSat-2 in the Norwegian Arctic to Field Measurements Made During the N-ICE2015 Expedition. J. Geophys. Res., 123(2), pp. 1123-1141.

Kwok, R. 2014. "Simulated Effects of a Snow Layer on Retrieval of CryoSat-2 Sea Ice Freeboard." Geophysical Research Letters 41: 5014–5020. https://doi.org/10.1002/2014GL060993.

Kwok, R., Kacimi, S., Markus, T., Kurtz, N.T., Studinger, M., Sonntag, J.G., Manizade, S.S., Boisvert, L.N. and Harbeck, J.P., 2019. ICESat-2 surface height and sea ice freeboard assessed with ATM lidar acquisitions from Operation IceBridge. Geophysical Research Letters, 46(20), pp.11228-11236.

Landy, J. C., Tsamados, M., & Scharien, R. K. (2019). A Facet-Based Numerical Model for Simulating SAR Altimeter Echoes From Heterogeneous Sea Ice Surfaces. *IEEE Transactions on Geoscience and Remote Sensing*, *57*(7), 4164–4180. https://doi.org/10.1109/tgrs.2018.2889763

Landy, J.C., Petty, A.A., Tsamados, M. and Stroeve, J.C., 2020. Sea ice roughness overlooked as a key source of uncertainty in CryoSat-2 ice freeboard retrievals. Journal of Geophysical Research: Oceans, 125(5), p.e2019JC015820.

Larue, F., Picard, G., Aublanc, J., Arnaud, L., Robledano-Perez, A., Meur, E.L., Favier, V., Jourdain, B., Savarino, J. and Thibaut, P., 2021. Radar altimeter waveform simulations in Antarctica with the Snow Microwave Radiative Transfer Model (SMRT). Remote Sensing of Environment, 263, p.112534.

Lawrence, I.R., T.W.K. Armitage, M.C. Tsamados, J.C. Stroeve, S. Dinardo, A.L. Ridout, A. Muir, R.L. Tilling, and A. Shepherd. 2019. "Extending the Arctic Sea Ice Freeboard and Sea Level Record with the Sentinel-3 Radar Altimeters." Advances in Space Research. https://doi.org/10.1016/j.asr.2019.10.011.

Lawrence, Isobel R., Michel C. Tsamados, Julienne C. Stroeve, Thomas W.K. Armitage, and Andy L. Ridout. 2018. "Estimating Snow Depth over Arctic Sea Ice from Calibrated Dual-Frequency Radar Freeboards." The Cryosphere 12 (11): 3551–64. https://doi.org/10.5194/tc-12-3551-2018.

Merkouriadi, I., Gallet, J. C., Graham, R. M., Liston, G. E., Polashenski, C., Rösel, A., & Gerland, S. (2017). Winter snow conditions on Arctic sea ice north of Svalbard during the Norwegian young sea ICE (N-ICE2015) expedition. *Journal of Geophysical Research: Atmospheres*, *122*(20), 10-837.

Nandan, V. et al., 2017. Effect of Snow Salinity on CryoSat-2 Arctic First-Year Sea Ice Freeboard Measurements. Geophys. Res. Lett., 44(20), p. 10419–10426.

Ricker, R. et al., 2015. Impact of snow accumulation on CryoSat-2 range retrievals over Arctic sea ice: An observational approach with buoy data. Geophys. Res. Lett., 42(11), pp. 4447-4455.

Shalina, E. V., Khvorostovsky, K., & Sandven, S. (2020). Arctic Sea Ice Thickness and Volume Transformation. In *Sea Ice in the Arctic* (pp. 167-246). Springer, Cham.

Stroeve, J., & Notz, D. (2018). Changing state of Arctic sea ice across all seasons. *Environmental Research Letters*, *13*(10), 103001.

Tilling, R., A. Ridout, and A. Shepherd. 2019. "Assessing the Impact of Lead and Floe Sampling on Arctic Sea Ice Thickness Estimates from Envisat and CryoSat-2." Journal of Geophysical Research: Oceans 124 (11): 7473–85. https://doi.org/10.1029/2019JC015232.

Warren, S. G., Rigor, I. G., Untersteiner, N., Radionov, V. F., Bryazgin, N. N., Aleksandrov, Y. I., & Colony, R. (1999). Snow depth on Arctic sea ice. *Journal of Climate*, *12*(6), 1814-1829.

Webster, M. A., Rigor, I. G., Nghiem, S. V., Kurtz, N. T., Farrell, S. L., Perovich, D. K., & Sturm, M. (2014). Interdecadal changes in snow depth on Arctic sea ice. *Journal of Geophysical Research: Oceans*, *119*(8), 5395-5406.

Willatt, R. et al., 2011. Ku-band radar penetration into snow cover on Arctic sea ice using airborne data. Ann. Glaciol., 52(57), pp. 197-205.

End of the document